Multi-Qubit Fuels

by

Angsar Manatuly

A Dissertation Submitted to the

Graduate School of Sciences and Engineering

in Partial Fulfillment of the Requirements for

the Degree of

Master of Science

in

Physics

KOÇ
UNIVERSITY

May 30, 2018

Multi-Qubit Fuels

Koç University

Graduate School of Sciences and Engineering

This is to certify that I have examined this copy of a master's thesis by

Angsar Manatuly

and have found that it is complete and satisfactory in all respects,

and that any and all revisions required by the final

examining committee have been made.

Committee Members:

_____

Prof. Dr. Özgür E. Müstecaplıoğlu (Advisor)

_____

Assoc. Prof. Dr. Alkan Kabakçıoğlu

_____

Asst. Prof. Dr. Ilke Ercan

Date: _____

ABSTRACT

In the last decade, there has been a major development to understand the properties of non-thermal baths, which can be used as a fuel for quantum heat engines. The efficiency of such engines can surpass the classical Carnot bound, and these engines can even operate with a single heat bath and an information reservoir. Quantum coherent particle clusters are one of the examples of such non-thermal baths. Decoherence is the major obstacle for utilizing the advantages of quantum coherent fuels. Increasing the number of particles and thus the amount of coherence can overcome this obstacle. However, the analytical studies of such non-thermal reservoirs were investigated only up to three coherent particles, and for the general coherent multi-particle fuels results were obtained numerically. In this thesis, we analytically show how coherences are classified in N-qubit clusters in terms of their interaction with the working fluid. We demonstrate that these coherent N-qubit clusters can thermalize, coherently drive the working mode, or can be used to engineer effective squeezed thermal bath. We show that the steady-state temperature of the working mode can scale linearly or quadratically with the number of the qubits in the cluster. We also construct an Otto engine using our model and show that we can increase efficiency bound. Finally, we propose how we can implement our model in a circuit-QED platform.

ÖZETÇE

Son on yılda, kuantum ısı motorları için yakıt olarak kullanılabilen termal olmayan rezervuarların özelliklerini anlamak için büyük bir gelişme olmuştur. Bu motorların verimliliği klasik Carnot sınırını aşabilir ve bu motorlar tek bir ısı rezervuarı ve bir bilgi deposuyla bile çalışabilir. Bu tür termal olmayan rezervuarların örneklerinden biride kuantum uyumlu parçacık kümeleridir. Kuantum uyumlu yakıtların avantajlarından yararlanmanın önündeki en önemli engel de eşevresizliktir. Parçacıkların sayısının artırılması ve dolayısıyla uyumluluğun artması bu engeli ortadan kaldırabilir. Bununla birlikte, bu tür termal olmayan rezervuarların analitik çalışmaları sadece üç tane uyumlu parçacığa kadar incelenmiş ve genel uyumlu çoklu parçacık yakıtlar için sonuçlar nümerik olarak elde edilmiştir. Bu tez çalışmasında, biz analitik olarak uyumluluğun N-qubit kümelerle, çalışma akışkanları ile etkileşimleri açısından, sınıflandırılabileceğini gösterdik. Bu uyumlu N-qubit kümelenmelerinin, çalışma modunu tutarlı bir şekilde hareket ettirebildiğini, ya da etkili sıkışmış termal rezervuarı kurmak için kullanılabileceğini gösteriyoruz. Çalışma modunun sabit durum sıcaklığının, kümedeki qubit sayısı ile doğrusal veya kuadratik olarak ölçeklenebileceğini göstermekteyiz. Modelimizi kullanarak bir Otto motoru da tasarlıyoruz ve verimlik sınırının artırabileceğimizi gösteriyoruz. Son olarak, modelimizi bir devre QED platformunda nasıl uygulayabileceğimizi öneriyoruz.

ACKNOWLEDGMENTS

I want to express my gratitude for my thesis advisor Professor Dr. Özgür E. Müstecaplıoğlu for supporting me and guiding me during my MS studies. I learned a lot and developed valuable research skills. Whenever I had some problems that I could not resolve, thanks to his advises and guidance I was able to progress on my projects consistently. He is not only a good research advisor, but also a nice person to work with.

I also want to thank Prof. Alkan Kabakçıoğlu and Prof. Ilke Ercan for accepting to be the jury committee and reviewing my thesis.

I want to thank Dr. Barış Çakmak for sharing his ideas and being a great collaborator. I appreciate his genuine support.

I am also grateful for my group mates. It has been fun to be together these two years. I want to thank Cahit Kargı and Dr. Ricardo Roman Ancheyta for their willingness to help whenever I asked them questions. I am grateful for Emre Köse and Serhat Can Kadıoğlu for helping me translate the abstract of the thesis into Turkish.

I want to acknowledge Ceren B. Dağ for her original idea of the coherent qubit clusters. Thanks to her work I could write my own thesis and obtain new results.

Finally, I am grateful for my family who always support me no matter what kind of decisions I make in my life.

TABLE OF CONTENTS

LIST OF TABLES

LIST OF FIGURES

NOMENCLATURE

$\hbar$:   Planck's constant

k_b: Boltzmann constant

Chapter 1

INTRODUCTION

1.1 Nonthermal Baths

Traditionally the dynamics of thermodynamic systems is described by the systems interacting with reservoirs at thermal equilibrium. However, this is an idealistic model. In fact, non-equilibrium systems are widely present in nature, some of the examples of such states being sunlight, biological cells, and laser light [1]. Over the past decade, a major development has been made to understand the dynamics of the systems interacting with non-equilibrium thermal baths. Non-equilibrium properties in reservoirs can arise because of multiple reasons. We cannot define a temperature for the bath if not all of the modes in the reservoir are at the same temperature. Also, reservoir cannot be in thermal equilibrium if a bath is spatially non-homogeneous. Moreover, quantum features such as quantum correlations, entanglement and coherences become more prominent in small-scale systems.

1.2 Quantum Heat Engines

These quantum features have essential role in Quantum heat engines [2]. Similar to its classical counterpart, QHE is a device that operates between hot and cold baths and extracts work from the heat flow. Since the engine is governed by the quantum mechanic laws, in order to enhance the efficiency it is important to take advantage of quantum features. For example, quantum correlations and entanglement can create a work output [3], and can be used to construct quantum heat engines [4, 5], enhancing efficiency and work [6]. Another difference of QHE from classical ones is that the efficiency of QHE can surpass the Carnot bound without violating thermodynamic laws.

Scully and collaborators showed this by proposing a photo-Carnot engine which uses quantum coherences as a resource [7]. The quantum systems are said to be coherent if there is a constant phase difference among them. Scully and collaborators introduced a fuel called phaseonium consisting of an ensemble of three-level atoms having coherence between its two ground states, and let this atoms interact one by one with the cavity field. As illustrated in Fig. 1.1, one of the mirrors moves due to light pressure and acts as a piston. The beam of three-level atoms act as a nonthermal reservoir. Therefore it is possible to extract work and build a Carnot engine using this system. They showed that the efficiency of the engine depends on the phase of the coherences and for a certain phase it can surpass the Carnot efficiency. It is even possible extract work from a single heat reservoir. This result later led to studies on quantum heat engines incorporating non-thermal reservoirs with quantum coherences [8, 9, 10].
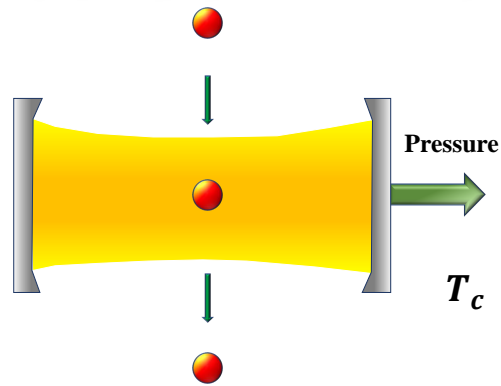
Figure 1.1: Quantum heat engine

1.3   *Coherent multi-qubit nonthermal baths*

Theoretical explanation of why the efficiency of such quantum heat engines can surpass Carnot limit is as follows. Carnot bound takes into account only heat transfer between thermal reservoirs, whereas non-thermal baths can transfer not only heat but also additional work to the working object [11]. In addition, coherences alter the temperature of the reservoir to a new effective one. Taking into account this new effective temperature, Carnot

bound should be redefined. These coherences can be used to create effective heat and work reservoirs. Coherences have a specific location in the density matrix of coherent qubit systems, and each location has a disjoint effect on the working mode. For example, nonthermal bath comprised of coherent three-qubit system can thermalize, coherently drive or create a squeezed field in the cavity [12, 13]. Considering thermalization coherences, when qubits were in symmetric W-states they increased the temperature significantly compared to the case without any coherences. GHZ states can even thermalize to an infinite temperature.

Main interest of this thesis is a non-thermal thermalization. Non-thermal baths incorporating quantum coherence can be obtained using single two-level [14], single three-level [7], two-particle [15], three-particle [12], and multi-particle [10, 16] systems. However, the analytical classification of coherences in terms of their disjoint contribution to the working mode was investigated only up to three particle systems [12], and for the general coherent multi-particle fuels results were obtained numerically. Therefore, there are no related reports analytically showing the classification of coherences for N qubit fuels. Furthermore, decoherence, which is the process of losing coherences, can be a major stumbling block to utilize the advantages of quantum coherences. Because of the non-ideal conditions, qubits interact with their surrounding environment and as a result of non-unitary dynamics, they irreversibly lose coherences. It was shown for the single three-level fuel case that if the quality factor of the cavity is not high then because of the dephasing quantum-classical transition occurs [17]. Increasing the amount of coherences can counter this effect. For example, as a generalization of the three-level phaseonium fuel case, N+1-level atom fuels with coherent N lower levels can beat decoherence [18]. The number of coherences scales quadratically N^2 for high N. In this case the decoherence is slower than quadratic increase of coherences for high N. Hence, we increase the amount coherences in the non-thermal fuel by using coherent N-atom fuels.

1.4 Our Model

In our system, we use single qubit instead of a micromaser as a working fluid as shown in Fig. 1.2. A beam of identically prepared coherent N-qubit clusters interacts with the

single qubit. The clusters arrive randomly and each cluster interacts with the qubit for a short time, and replaced by the next cluster. Single-atom engines have already been proposed and experimentally realized using ion traps [19, 20, 21]. Homogeneity is the main advantage of our system. Both non-thermal bath and the working fluid are realized using qubits and therefore there is no interface challenge.
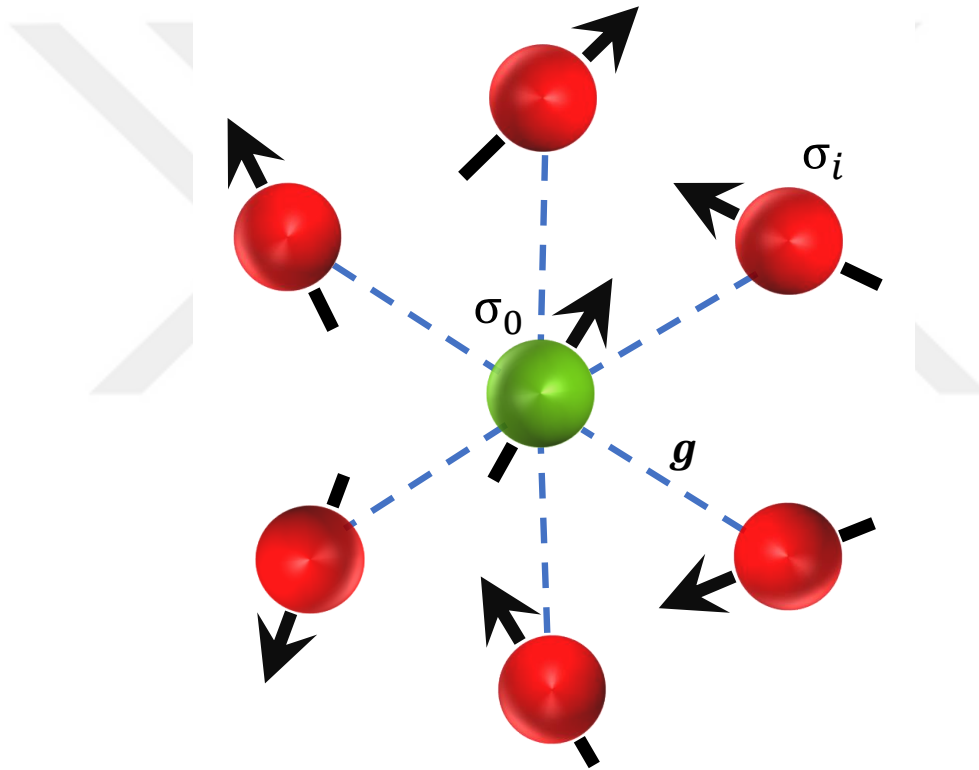
Figure 1.2: N-qubit fuel interacting the single qubit

Another possible way to realize the system experimentally is Circuit QED [22, 23, 24]. This thesis shows that coherent N-qubit fuel depending on the type of coherences can behave as a squeezed bath, coherently drive the qubit, or thermalize the qubit to a certain temperature. These coherences are classified according to their locations in the density matrix of the N-qubit fuel. For instance, the coherences which thermalize the working qubit classified as heat exchange coherences (HEC) are located along the main diagonal in the Wigner-Jordan blocks. We show analytically the dependence of the thermalization

temperature of the working fuel on the number of the qubits in the cluster is quadratic, thus verifying previous numerical approximations [10]. In addition, it is possible to engineer squeezed thermal bath using our model. In chapter 2 we derive the master equation for a small number of qubits, namely two, three and four-qubit cases. We show how coherences are classified, and see that there is a certain pattern for location of these coherences in the density matrix of the qubit cluster. In chapter 3 we generalize this result to N-qubit case, and verify that the coherences are located with a specific pattern. In chapter 4 we show how heat exchange coherences can be thermally generated. In chapter 5 we investigate how to harvest heat exchange coherences and how they thermalize the working qubit. In chapter 6 we show how effective squeezed thermal bath can be engineered using qubits only. In chapter 7 we construct the Otto engine using our model and analyze its efficiency. In chapter 8 we present circuit QED system to implement our model.

Chapter 2

PRELIMINARY

The classification of coherences in terms of their disjoint contribution to the working fluid has already been obtained [12] for the multi-qubit fuels with up-to three qubits. Before obtaining the generalized result for N qubit cluster, here we try to reproduce the master equation for the cases of two, three and four coherent qubit clusters. Clusters of coherent qubits repeatedly interact with single working qubit at random time intervals. The clusters arrive randomly to the single qubit with the rate p.

Coherent Qubit Pair Fuel

Qubit pairs arrive randomly at a rate **p**

Working Qubit
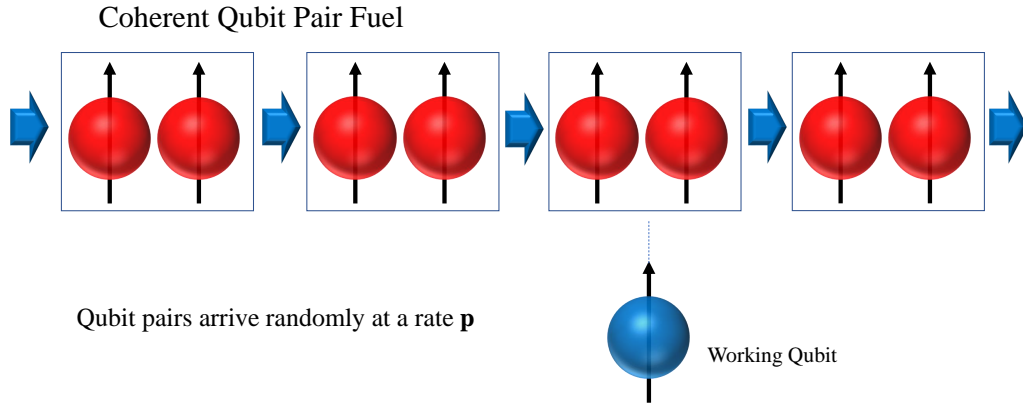
Figure 2.1: This is an example of our model for the case of coherent two-qubit fuel

We assume ideal environment conditions ignoring atomic dephasing and relaxation. Each clusters have a density matrix ρ_f before interaction, and the single qubit has ρ_q. During interaction the total density matrix is given as $\rho(t) = \rho_f(t) \bigotimes \rho_q(t)$. We assume that all the qubits have the same transition frequency ω. Then the interaction is governed by the total Hamiltonian which is given as

$$H = H_q + H_f + H_{\text{int}} \tag{2.1}$$

where the first, second and third terms

$$H_{\mathrm{q}} = \frac{\hbar\omega}{2}\sigma_0^z,$$

$$H_{\mathrm{f}} = \sum_{i=1}^{N} \frac{\hbar\omega}{2}\sigma_i^z,$$

$$H_{\mathrm{int}} = \hbar g \sum_{i=1}^{N}(\sigma_i^+ \sigma_0^- + \sigma_i^- \sigma_0^+)$$

(2.2)

are working qubit, N-qubit cluster, and interaction Hamiltonians respectively. Operators $\sigma_i^z, \sigma_i^+, \sigma_i^-$ are Pauli z, raising and lowering operators respectively. The interaction is a dipole-dipole. We assumed that the working qubit interacts with the same interaction strength g with each qubit in the cluster. We move to the interaction picture, and the evolution is governed by the time-evolution propagator $U(\tau) = \exp(-iH_{\mathrm{int}}\tau)$, where τ is the interaction time. We use another assumption that the interaction is short time such that $g\tau << 1$. Under this assumption, the propagator can be expressed to the second order and the examples for two and three-qubit cases are given in the Appendix A.

Because of the randomness of the interactions the evolution of the total density matrix during time δt has two possibilities, it either changes or stays constant which is described as [13].

$$\rho(t + \delta t) = p\delta t U(\tau)\rho(t)U^\dagger(\tau) + (1 - p\delta t)\rho(t)$$

(2.3)

The master equation of the total density matrix in the limit $\delta t \to 0$ is obtained as

$$\dot{\rho}(t) = p(U(\tau)\rho(t)U^\dagger(\tau) - \rho(t)).$$

(2.4)

We can obtain the master equation for the qubit by tracing out the cluster qubit density matrix

$$\dot{\rho}_q(t) = p\Big[\sum_{i,j=1}^{N} a_{ij} \sum_{n=1}^{N} U_{ni}(\tau)\rho_q(t)[U_{nj}(\tau)]^\dagger - \rho_q(t)\Big],$$

(2.5)

where a_{ij} are the density matrix elements of the qubit cluster $\rho_f(t)$. $U_{ni(j)}$ are the matrix elements of the time-evolution propagator $U(\tau)$. Expanding U_{ni} and U_{nj} we find that the master equation can be written as

$$\dot{\rho}_q(t) = -i[H_{eff}, \rho_q] + \mathcal{L}_s\rho_q + \mathcal{L}_h\rho_q$$

(2.6)

where the terms in the master equation are given as

$$H_{\text{eff}} = pg\tau(\lambda\sigma_0^+ + \lambda^*\sigma_0^-)$$

$$\mathcal{L}_s\rho = \mu(\epsilon\sigma_0^+\rho_q\sigma_0^+ + \epsilon^*\sigma_0^-\rho_q\sigma_0^-) \tag{2.7}$$

$$\mathcal{L}_h\rho = \mu\frac{r_d}{2}[2\sigma_0^-\rho_q\sigma_0^+ - \sigma_0^+\sigma_0^-\rho_q - \rho_q\sigma_0^+\sigma_0^-] + \mu\frac{r_e}{2}[2\sigma_0^+\rho_q\sigma_0^- - \sigma_0^-\sigma_0^+\rho_q - \rho_q\sigma_0^-\sigma_0^+]$$

and $\mu = p(g\tau)^2$. We can observe that each terms in master equation corresponds to a specific interaction type of the heat bath and the working mode. The first term corresponds to the effective driving of the qubit with coherent field. The second term is the effective coupling of the qubit with the squeezed bath. The third term is the effective interaction of the qubit with the thermal bath. Coefficients of the effective Hamiltonian and the Lindbladians depend on the location of the off-diagonal coherences of the qubit cluster and hence classified accordingly. Table 2.1 shows coefficients for two-qubit fuel. The Appendix B contains coefficients for three and four-qubit fuels, and Fig. 2.2 illustrates the density matrices.

r_e	$2a_{11} + a_{22} + a_{23} + a_{32} + a_{33}$
r_d	$2a_{44} + a_{22} + a_{23} + a_{32} + a_{33}$
λ	$a_{12} + a_{13} + a_{24} + a_{34}$
ϵ	a_{14}

Table 2.1: The Lindbladian coefficients in the master equation for two-qubit fuel case

(a) 4-qubit fuel

(b) 3-qubit fuel

(c) 2-qubit fuel
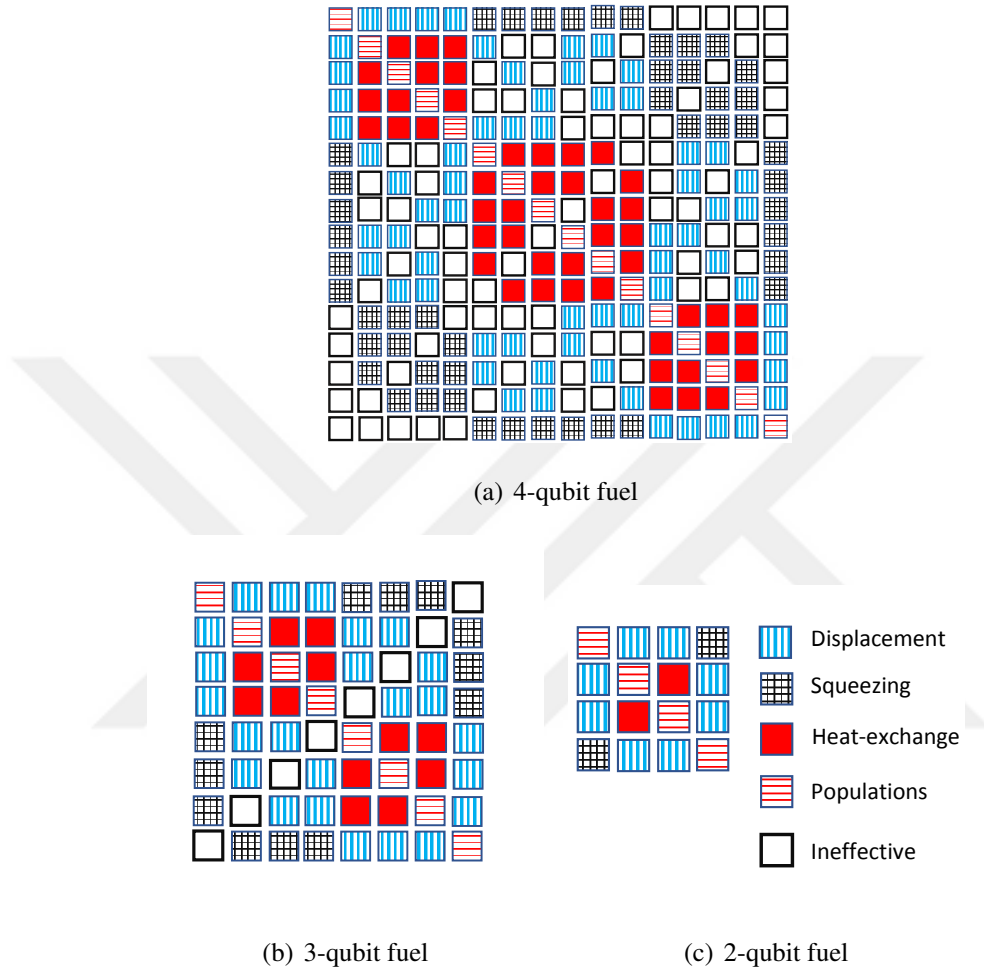
Figure 2.2: Density matrices of the qubit clusters in the computation basis

From Fig. 2.2 we can observe that there is a clear pattern for location of the coherences. The density matrices are defined in computation basis as shown in Fig. 2.3 to illustrate this. In this basis, the top left entry is related with the most excited states. As we go down along the diagonal, the number of excitations in the entries decreases, and the bottom right corner entry is related to the ground state.

Coherences have a disjoint contribution to the master equation. The main diagonal block matrices are associated with heat exchange coherences (HECs). HECs couple the states with the same energy and they contribute to $\mathcal{L}_h \rho$. The blocks adjacent to the main diagonal ones are related with displacement coherences. Displacement coherences cou-

$$\underline{e_1\, e_2\, e_3 \cdots e_{n-1}\, e_n}$$

$$\underline{e_1\, e_2\, e_3 \cdots e_{n-1}\, g_n} \qquad \underline{e_1\, e_2\, e_3 \cdots g_{n-1}\, e_n} \qquad \cdots \qquad \underline{g_1\, e_2\, e_3 \cdots e_{n-1}}$$

$$\underline{e_1\, e_2\, e_3 \cdots g_{n-1}\, g_n} \qquad \underline{e_1\, e_2 \cdots g_{n-2}\, g_{n-1}\, e_n} \qquad \cdots \qquad \underline{g_1\, g_2\, e_3 \cdots e_{n-1}}$$

$$\cdots$$

$$\cdots$$

$$\underline{g_1\, g_2\, g_3 \cdots g_{n-1}\, g_n}$$

Figure 2.3: The energy levels of the fuel qubits.

ple the states differing by one excitation contribute to and they contribute to H_{eff}. The blocks adjacent to the displacement coherences are associated with squeezing coherences. Squeezing coherences couple the states differing by two excitations and they contribute to $\mathcal{L}_s \rho$. Ineffective coherences cannot contribute to the master equation.

COHERENT N-QUBIT FUEL

From the density matrices obtained for 2-4 coherent fuels we cannot make a general statement about the classification and location of coherences for larger clusters. For this case, a general master equation is needed. Fig. 1.2 illustrates our model. This a central spin model [25], and is the special case of the Gaudin spin model [26]. In order to derive the master equation we use collective spin operators. The interaction Hamiltonian is given as

$$H_{\text{int}} = \hbar g \sum_{i=1}^{N} (\sigma_i^+ \sigma_0^- + \sigma_i^- \sigma_0^+) = \hbar g (J_+ \sigma_0^- + J_- \sigma_0^+), \qquad (3.1)$$

where $\sigma_i^- = |g_i\rangle\langle e_i|$, $\sigma_i^+ = |e_i\rangle\langle g_i|$ are lowering and raising Pauli operators and $J_\pm = \sum_{i=1}^{N} \sigma_i^\pm$ are collective raising and lowering spin operators of the N qubit cluster which expresses the fact that qubits inside the fuel clusters interact collectively with the working qubit in the specified time interval. Eq. (3.1) is directly or effectively applicable to various systems involving central spin models. For example, it can be used to describe nuclear spin baths in quantum dots [27, 28], nitrogen-vacancy center [29], and nuclear magnetic resonance systems [30]. This model can also be used to describe effective spin systems in coupled microcavities [31, 32], and coupling in superconducting qubits [33, 34], and molecular nanomagnets [35, 36].

We consider the evolution of the system in the interaction picture associated with the self-Hamiltonians, H_q and H_f, and the total system evolves unitarily during interaction time τ by the propagator $U(\tau) = \exp(-iH_{\text{int}}\tau/\hbar)$, which can be expressed as follows

$$\begin{aligned} U \approx \mathbb{1} &- ig\tau(J_+ \sigma_0^- + J_- \sigma_0^+) \\ &- \frac{(g\tau)^2}{2}(J_+ J_- \sigma_0^- \sigma_0^+ + J_- J_+ \sigma_0^+ \sigma_0^-), \end{aligned} \qquad (3.2)$$

up to second order in $g\tau$. Before each interaction, the total density matrix of the working qubit and atomic cluster can be written as the product of two $\rho(t) = \rho_f(t) \bigotimes \rho_q(t)$. From now on we drop zero subscript in the Pauli matrices of the working qubit. Since the working qubit interacts randomly with the fuel qubits at a rate p, in a given time interval δt, $\rho(t)$ either evolves under Eq. (3.2) or remains intact

$$\rho(t + \delta t) = p\delta t U(\tau)\rho(t)U^\dagger(\tau) + (1 - p\delta t)\rho(t). \tag{3.3}$$

In the limit $\delta t \to 0$, the master equation describing the dynamics of the working qubit can be obtained by tracing out the degrees of freedom of atomic cluster

$$\dot{\rho}_q(t) = \text{Tr}_f[p(U(\tau)\rho(t)U^\dagger(\tau) - \rho(t))]$$
$$= -i[H_{\text{eff}}, \rho_q] + \mathcal{L}_s\rho_q + \mathcal{L}_h\rho_q, \tag{3.4}$$

where the effective Hamiltonian, H_{eff}, and Lindblad dissipators in the master equation are given as

$$H_{\text{eff}} = pg\tau(\lambda\sigma^+ + \lambda^*\sigma^-),$$
$$\mathcal{L}_s\rho = \mu(\epsilon\sigma^+\rho_q\sigma^+ + \epsilon^*\sigma^-\rho_q\sigma^-),$$
$$\mathcal{L}_h\rho = \mu\frac{r_d}{2}[2\sigma^-\rho_q\sigma^+ - \sigma^+\sigma^-\rho_q - \rho_q\sigma^+\sigma^-], \tag{3.5}$$
$$+ \mu\frac{r_e}{2}[2\sigma^+\rho_q\sigma^- - \sigma^-\sigma^+\rho_q - \rho_q\sigma^-\sigma^+],$$

with $\mu = p(g\tau)^2$ and the coefficients are presented in Table 3.1.

r_e	$\langle J_+ J_- \rangle$
r_d	$\langle J_- J_+ \rangle$
λ	$\langle J_- \rangle$
ϵ	$\langle J_- J_- \rangle$

Table 3.1: The Lindbladian coefficients in the master equation

We describe the density matrix in the computational basis $\{|e_1e_2 \ldots e_{n-1}e_n\rangle, |e_1e_2 \ldots e_{n-1}g_n\rangle, |e_1e_2 \ldots g_{n-1}e_n\rangle, \ldots, |g_1g_2 \ldots g_{n-1}g_n\rangle\}$. Derived master equation for general case confirms the results from previous chapter about the classification of coherences according to

their location. The unitary dynamics induced by H_{eff}, couples states differing by one excitation and elements of ρ_f that are involved in this process are called displacement coherences. The physical mechanism coupling the states differing by two excitations is described by $\mathcal{L}_s \rho$ where the coherences associated with it are called squeezing coherences. Finally, physical processes coupling states at the same energy that induce an emission or absorption processes are due to $\mathcal{L}_h \rho$ and associated coherences are labeled as heat-exchange coherences (HECs).

Let us describe HECs in a more detail. They are located in the off-diagonals of $C(N, k) \times C(N, k)$ sized blocks running through the main diagonal of ρ_f, with N being the number of fuel qubits and $k = 0, 1, \ldots, N$ is the number of excitations and presented as solid red squares in Fig. 3.1.
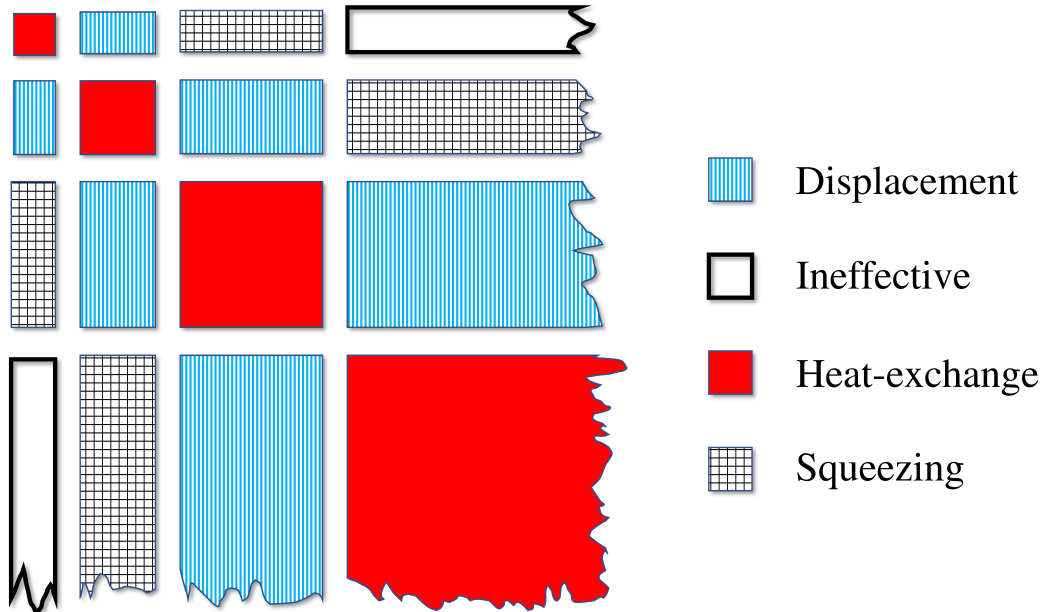
Figure 3.1: Density matrix of the fuel qubits in the computation basis. As described by the master equation in Eq. (3.4) each state of the fuel qubit has specific role in the evolution of the working qubit. The main diagonal squares are the states representing heat-exchange coherences and populations that thermalize the working qubit. Squares with vertical lines are the displacement coherences, and squares with grid are the squeezing coherences.

These blocks are known as Jordan-Wigner or Dicke blocks in the density matrix and number of them together with their size can be determined by looking at the Pascal's triangle depicted in Fig. 3.2. On the other hand, displacement and squeezing coherences which are located between the states differing single and double excitations are presented in squares with blue vertical stripes and grids, respectively. However, there are certain elements that do not have any effect on the final state of the working qubit. These elements can both be present in the specified blocks or outside of them and they are called ineffective coherences and depicted as blank white squares.
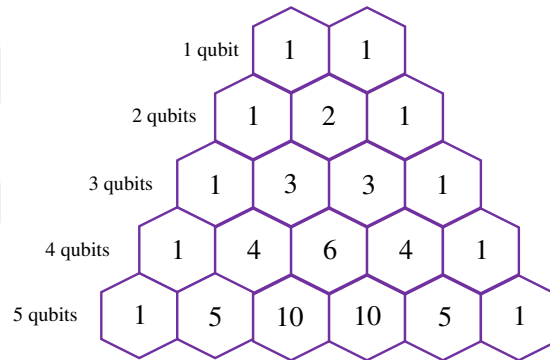
Figure 3.2: For each number of N-qubit fuels we can find the size of the HECs blocks from Pascal's triangle. The size for 1-5 qubit clusters is shown here, and for higher number of clusters the dimension of HECs blocks can be calculated similarly.

Chapter 4

THERMAL GENERATION OF HEAT EXCHANGE COHERENCES

We present here how HECs can be generated from a thermal environment. By collective coupling to the thermal environment an ensemble of two-level atoms, it is possible to generate heat-exchange coherences [37]. This is possible only when the average distance between clusters is less than the wavelength of the photons in the heat bath. We can use this model in the present case.
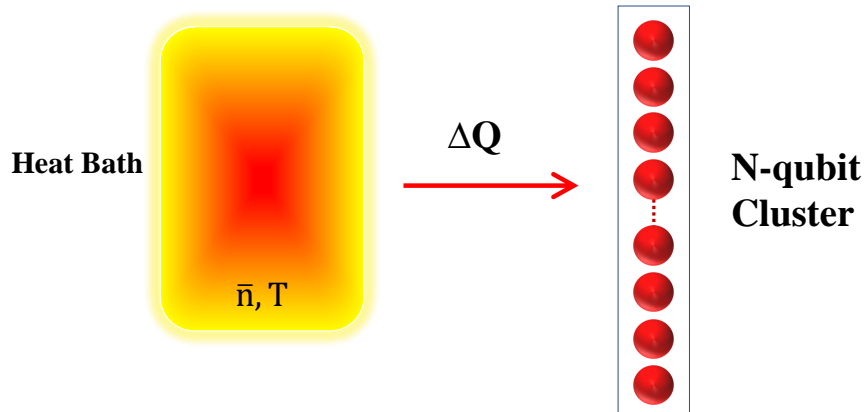
Figure 4.1: Thermal generation of the HECs in N-qubit cluster

The master equation in the interaction picture associated with respect to the self-Hamiltonians of the qubits in the cluster is given in the standard Lindblad form as

$$\frac{d\rho_f}{dt} = \mathcal{L}(\rho_f) = \mathcal{D}_-(\rho_f) + \mathcal{D}_+(\rho_f).$$

(4.1)

The terms on the right-hand side will be specified below. The aforementioned collective

coupling to the thermal reservoir is possible only when the constituents of the fuel cluster are spatially close to each other. In this limit, it is possible to express the dissipators in Eq. (4.1) in terms of the collective spin operators and they have the following form

$$
\begin{aligned}
\mathcal{D}_-(\rho_f) &= \gamma_0(\bar{n}+1)(J_-\rho_f J_+ - \frac{1}{2}\{J_+J_-, \rho_f\}), \\
\mathcal{D}_+(\rho_f) &= \gamma_0\bar{n}(J_+\rho_f J_- - \frac{1}{2}\{J_-J_+, \rho_f\}),
\end{aligned}
\tag{4.2}
$$

where γ_0 is the spontaneous emission rate, $\bar{n}$ is the mean number of photons at a given temperature determined by the Planck distribution and $\mathcal{D}_-$ and $\mathcal{D}_+$ describe thermally induced emission and absorption processes, respectively.

We now present an analytical method to calculate the steady state, again for the ground initial state, for any number of qubits $\rho_f(t=0) = |g_1g_2\ldots g_N\rangle\langle g_1g_2\ldots g_N|$. Observe that, with a master equation consisting of dissipators involving absorption and emission processes, such as the ones given in Eq. (4.2), it is only possible to populate the Dicke blocks of the density matrix in the steady state which are nothing but the HECs. In this case, we can write the time evolved state of the system as follows

$$
\rho_f = \begin{pmatrix}
D_{N+1} & 0 & \ldots & 0 & 0 \\
0 & D_N & \ldots & 0 & 0 \\
\vdots & \vdots & \ddots & \vdots & \vdots \\
0 & 0 & \ldots & D_2 & 0 \\
0 & 0 & \ldots & 0 & D_1
\end{pmatrix}.
\tag{4.3}
$$

Here, D_i is the Wigner-Jordan block matrix, which can be decomposed as follows $D_i = d_iU_i$ with U_i being the matrix of ones and d_i is its entries. U_i has the dimension $p_i \times p_i$, and $p_i = C(N, i-1)$ corresponds to the ith element in the Pascal's triangle for particular N. For example, in case of $i = 1$, $U_1 = 1$ is the ground state, and d_1 is the population of all the qubits in the ground state. Together with the normalization condition

$$
\mathrm{Tr}(\rho_f) = \sum_{i=1}^{N+1} \mathrm{Tr}[D_i] = 1,
\tag{4.4}
$$

and making use of the identity $\mathrm{Tr}[D_{i+1}] = (\bar{n}/(\bar{n}+1))\mathrm{Tr}[D_i]$, which is proven in Ap-

pendix C, we can find the elements of the Wigner-Jordan blocks d_i's as follows

$$d_i = \frac{(1-r)r^{i-1}}{(1-r^{N+1})p_i},$$ (4.5)

where $r = \bar{n}/(\bar{n}+1)$. Therefore, we have shown that it is possible to extend the scheme proposed previously in [37], to generate N-qubit fuels for any N, by coupling them to a thermal reservoir in order to manipulate the state of a working qubit.

Chapter 5

HARVESTING HEAT EXCHANGE COHERENCES

5.1 Effective Thermalization of the Working Qubit

We introduce our harvesting scheme of HECs. Since these states contain non-zero elements only in the Dicke blocks through the main diagonal as shown in Fig. 3.1 and zero squeezing and displacement coherences $\epsilon = \lambda = 0$, the master equation derived for the evolution of the working qubit upon randomly interacting with N-qubit fuel clusters in Eq. (3.4) takes the form

$$
\dot{\rho}_q(t) = \mu \frac{r_d}{2} [2\sigma^- \rho_q \sigma^+ - \sigma^+ \sigma^- \rho_q - \rho_q \sigma^+ \sigma^-] +
$$
$$
+ \mu \frac{r_e}{2} [2\sigma^+ \rho_q \sigma^- - \sigma^- \sigma^+ \rho_q - \rho_q \sigma^- \sigma^+]. \tag{5.1}
$$

The steady-state solution of the above equation is calculated to be

$$
\rho_{\text{ss}} = \frac{1}{r_e + r_d} \begin{pmatrix} r_e & 0 \\ 0 & r_d \end{pmatrix}. \tag{5.2}
$$

From here, using Kubo-Martin-Schwinger (KMS) detailed-balance condition [38], we can define the effective temperature of the working qubit as

$$
T_q = -\frac{\hbar\omega}{k_b ln(\frac{r_e}{r_d})}, \tag{5.3}
$$

which explicitly depends on the HECs of the fuel qubits. The effective temperature of the qubit is positive if $r_d > r_e$. The working qubit is not in thermal equilibrium with the coherent qubit clusters, but it is in thermal equilibrium with the effective environment [12] described by the master equation Eq. 5.1. If we assume that this effective environment is consisted of harmonic oscillators, we can also define the average photon number of this bath as

$$
\bar{n} = \frac{1}{\exp(\frac{\hbar\omega}{k_b T_q}) - 1}. \tag{5.4}
$$

5.2   Simulation of the Interaction of the Cluster with the Qubit

Here we present the simulation in Python of the interaction of the cluster with the working qubit in order to show how the effective temperature of the qubit evolves. We choose clusters consisting of two coherent qubits as shown in Fig. 2.1. These coherent pair qubits are in thermal equilibrium at temperature $T = 3.22K$. We assume that the pairs arrive regularly without randomness and that there is no dephasing and decay in the qubits. The transition frequency of all of the qubits is the same $\omega = 6.4$GHz. The interactions strength is $g = 42$MHz, and the interaction time is $\tau = 1ns$. Since the qubit's density matrix is always diagonal, we can define the effective temperature of the qubit as in Eq. 5.3. We plot this effective temperature vs. time graph.
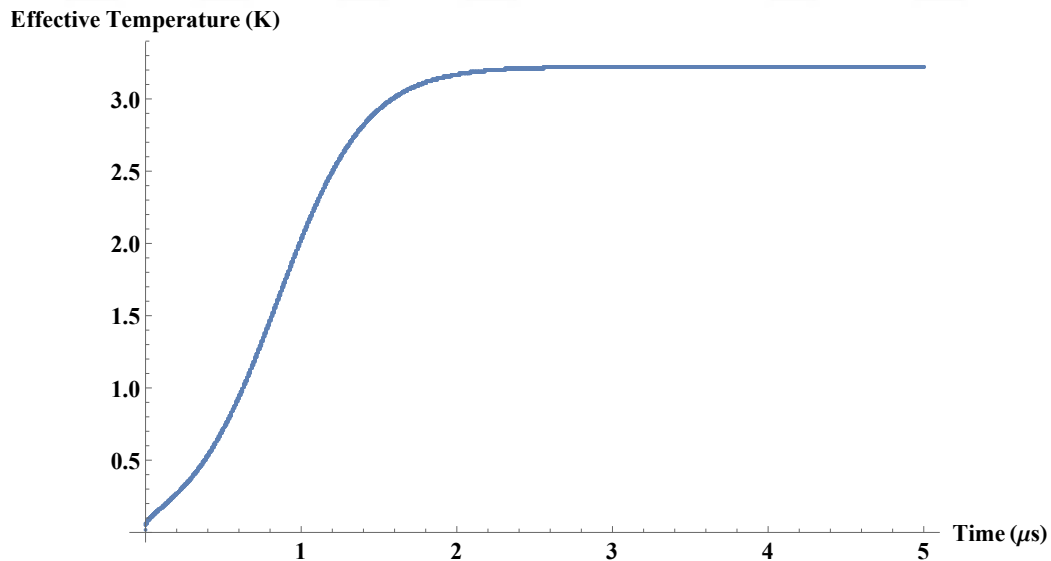
Figure 5.1: Evolution of the effective temperature of the qubit

From the above figure we cannot say exactly that the qubit reaches a steady-state, but its effective temperature approaches the temperature of the coherent qubit pairs quickly. This shows that the clusters increase the effective temperature of the qubit fast.

5.3 Thermally Generated Fuel

We are now going to introduce our harvesting scheme of the fuel clusters generated by the method introduced in the previous Chapter 4. Since these states contain non-zero elements only in the Dicke blocks through the main diagonal as shown in Fig. 3.1 and zero squeezing and displacement coherences, we calculate excitation r_e and de-excitation r_d coherences. Using block diagonal shape of the density matrix of the fuel qubits given in Eq. (4.3), we can find the populations of ρ_{ss}, from by calculating the expectation values shown in Table 3.1 as

$$
\begin{aligned}
r_e =& \text{Tr}[J_-\rho_f J_+] = \sum_{i=1}^{N+1} d_i \text{Tr}[J_- U_i J_+] \\
=& \sum_{i=1}^{N+1} d_i (N-i+2)^2 p_{i-1} \\
=& \sum_{i=1}^{N} \frac{(1-r)ir^i(N-i+1)}{(1-r^{N+1})},
\end{aligned}
\tag{5.5}
$$

and

$$
\begin{aligned}
r_d =& \text{Tr}[J_+\rho_f J_-] = \sum_{i=1}^{N+1} d_i \text{Tr}[J_+ U_i J_-] \\
=& \sum_{i=1}^{N+1} d_i i^2 p_{i+1} \\
=& \sum_{i=1}^{N} \frac{(1-r)ir^{i-1}(N-i+1)}{(1-r^{N+1})}.
\end{aligned}
\tag{5.6}
$$

Then, their ratio can be calculated as

$$
\frac{r_e}{r_d} = \frac{\bar{n}}{(\bar{n}+1)} = r.
\tag{5.7}
$$

From KMS detailed balance condition we can define the temperature of the working qubit as $T = -\hbar\omega/(k_b ln(r))$. It can be seen that this temperature is independent of the number of fuel qubits and is only dependent on the average number of photons $\bar{n}$ in the environment where fuel qubits were prepared. This leads us to the conclusion that the coherences created due to coupling with thermal photons, can only reflect the temperature of that environment

to the working qubit. Under this circumstances, there is no direct quantum advantage provided by fuel qubits prepared in this setup.

5.4   Thermally Entangled Fuel
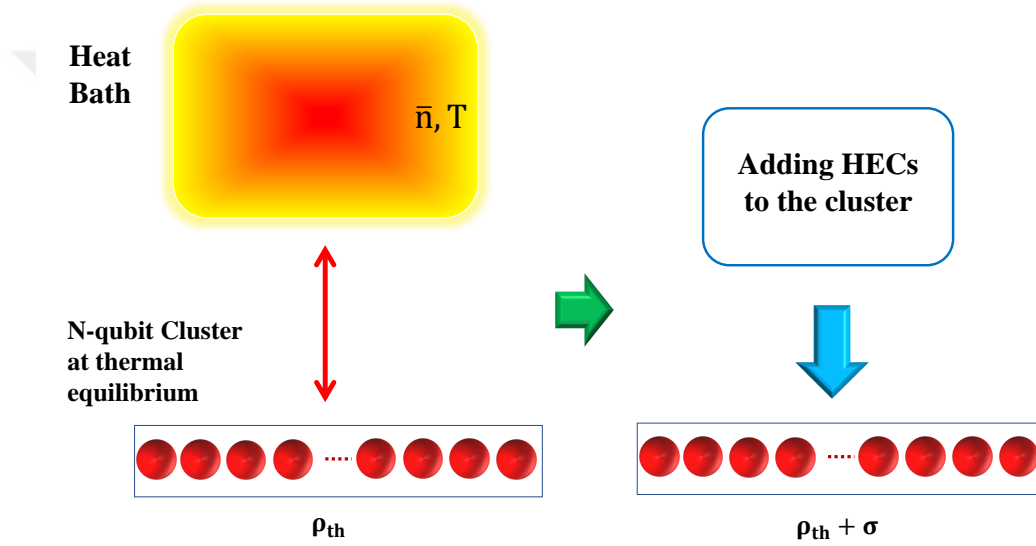
Figure 5.2: Thermally entangled fuel is created by adding HECs to the cluster at thermal equilibrium

We consider the N-qubit fuel formed by adding HECs coherences to the N-qubit cluster at thermal equilibrium. The density matrix will be block diagonal in this case too. It has the same structure as given in Eq. (4.3), and can be expressed as $\rho_f = \rho_{\text{th}} + \sigma$. The first term ρ_{th} corresponds to the density matrix of the cluster if it were in thermal equilibrium, and the second term σ is the HECs. This kind of fuel is a generalized form of a thermally entangled pair of qubits [5]. We consider adding σ such that each block D_i has the same entries. The blocks are expressed as $D_i = d_i U_i$. Since ρ_{th} is thermal, the relation $d_{i+1}/d_i = \bar{n}/(1+\bar{n}) = r$ holds, where $\bar{n}$ is the number of photons corresponding to the temperature of the ρ_{th}. The normalization condition gives

$$d_i = \frac{r^{i-1}}{(1+r)^N}. \tag{5.8}$$

The interaction of this fuel and the working qubit is governed by Eq. (5.1), and the qubit's final state is the same as Eq. (5.2). We calculate the populations of the qubit using the expectation values given in Table 3.1 as

$$
\begin{aligned}
r_e &= \mathrm{Tr}[J_-\rho_f J_+] = \sum_{i=1}^{N+1} d_i \mathrm{Tr}[J_- U_i J_+] = \\
&= \sum_{i=2}^{N+1} \frac{r^{i-1}(N-i+2)N!}{(1+r)^N(i-2)!(N-i+1)!} = \\
&= \frac{r(N+r)N}{(1+r)^2},
\end{aligned}
\tag{5.9}
$$

and

$$
\begin{aligned}
r_d &= \mathrm{Tr}[J_+\rho_f J_-] = \sum_{i=1}^{N+1} d_i \mathrm{Tr}[J_+ U_i J_-] = \\
&= \sum_{i=1}^{N} \frac{r^{i-1}iN!}{(1+r)^N(i-1)!(N-i)!} = \\
&= \frac{N(1+rN)}{(1+r)^2}.
\end{aligned}
\tag{5.10}
$$

Using the ratio of the populations r_e/r_d, and KMS detailed balance condition we can express define the steady-state temperature as

$$
T = -\frac{\hbar\omega}{k_b ln(\frac{r(N+r)}{1+Nr})}.
\tag{5.11}
$$

At high number of qubits we can obtain the temperature as

$$
T \approx \frac{\hbar\omega(1+Nr)}{k_b(1-r^2)} \approx \frac{\hbar\omega Nr}{k_b(1-r^2)}.
\tag{5.12}
$$

The temperature increases linearly as the number of the qubits increases. This is expected because we added HECs coherences to the cluster which was at thermal equilibrium. It costs additional energy to add HECs, therefore it is reasonable that temperature of the working qubit will be larger than the temperature of the cluster at thermal equilibrium ρ_{th}.

5.5 Athermal Fuel

5.5.1 Ideal Environment Case

Let us consider the N-qubit fuel having a density matrix such that only single Wigner-Jordan block is non-zero, and all other blocks are zero.

$$\rho_m = \begin{pmatrix} 0 & 0 & \dots & 0 & 0 & 0 \\ 0 & 0 & \dots & 0 & 0 & 0 \\ & & \dots & & & \\ 0 & 0 & D_m & 0 & 0 & 0 \\ & & \dots & & & \\ 0 & 0 & \dots & 0 & 0 & 0 \\ 0 & 0 & \dots & 0 & 0 & 0 \end{pmatrix}. \tag{5.13}$$

We assume that D_m matrix has entries which are all equal to each other, and from normalization condition it can be expressed as

$$D_m = \frac{1}{p_m} U_m \tag{5.14}$$

where p_m is the dimension of the Wigner-Jordan block and equal to the corresponding element in Pascal's triangle. Similar to the thermal fuel case, in order to determine the steady-state temperature, we again calculate r_e and r_d using the form of ρ_f given in Eq. (5.13) as

$$r_e = \frac{1}{p_m} \text{Tr}[J_- U_m J_+] = \frac{1}{p_m}(N - m + 2)^2 \binom{N}{m-2},$$
$$r_d = \frac{1}{p_m} \text{Tr}[J_+ U_m J_-] = \frac{1}{p_m} m^2 \binom{N}{m}. \tag{5.15}$$

So that their ratio is given as

$$\frac{r_e}{r_d} = \frac{(N-m)m + 3m - N - 2}{(N-m)m + m} = 1 + \frac{2m - N - 2}{(N-m)m + m}. \tag{5.16}$$

From KMS condition, we can define the steady state temperature of the working qubit as follows

$$T = -\frac{\hbar\omega}{k_b ln\left(\frac{(N-m)m+3m-N-2}{(N-m)m+m}\right)}. \tag{5.17}$$

One thing that we can immediately observe is that the final temperature depends on the location of the D_m. For example, if $m = 1$ which corresponds to the ground state, the final temperature will be zero. When it is located around the center, in the limit of large fuel clusters, i.e. large N, the effective temperature of the working qubit can be approximated as

$$T \approx \frac{\hbar\omega}{k_b} \frac{(N-m)m + m}{N - 2m + 2}. \tag{5.18}$$

In contrary to the case where the coherences are thermally distributed, the scaling is quadratic with the size of the fuel clusters when we have non-thermally distributed coherence blocks. We can observe that if Wigner-Jordan block is located on the lower half $m < (N+2)/2$ the temperature is positive, and if it is on the upper side it becomes negative.
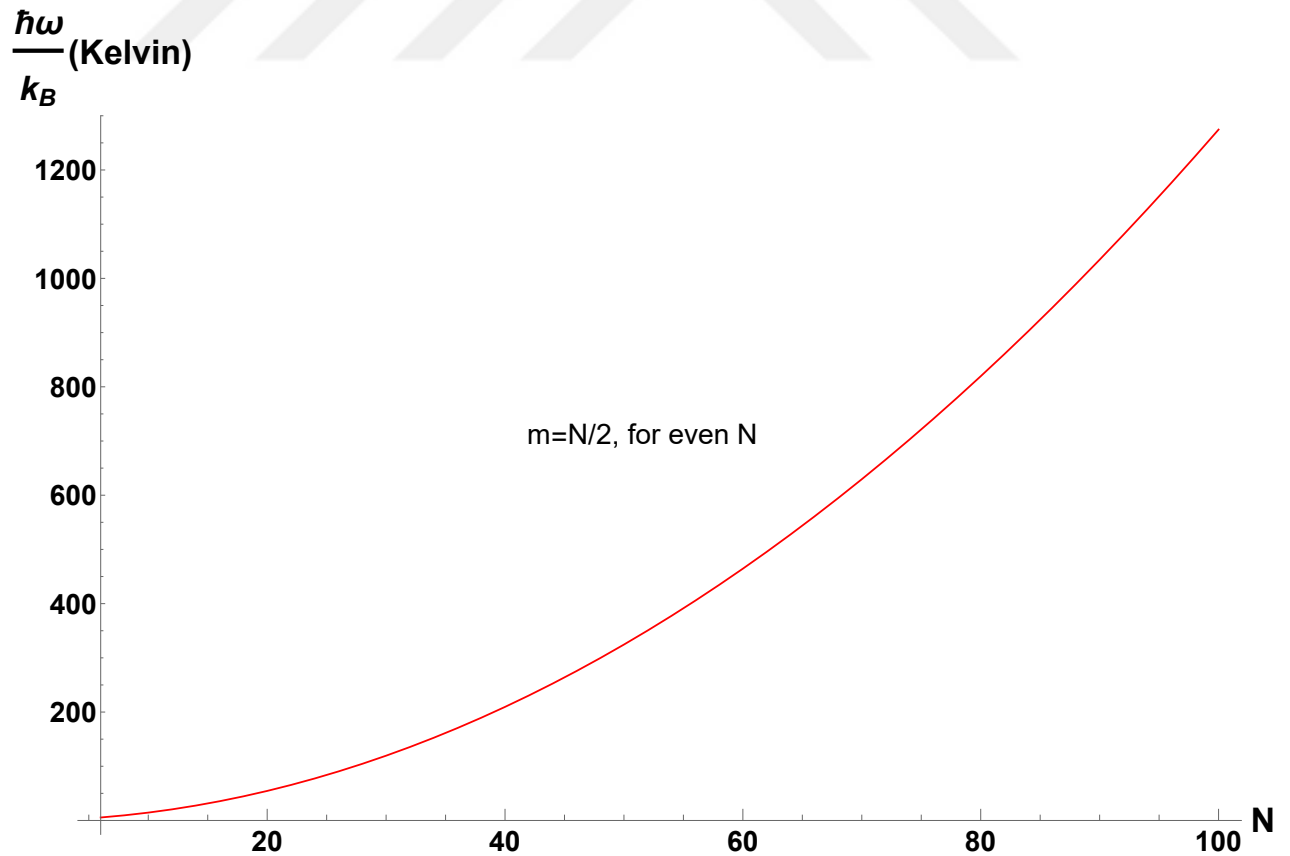
Figure 5.3: Effective temperature scaling for $m = N/2$, and even number of qubits in the cluster
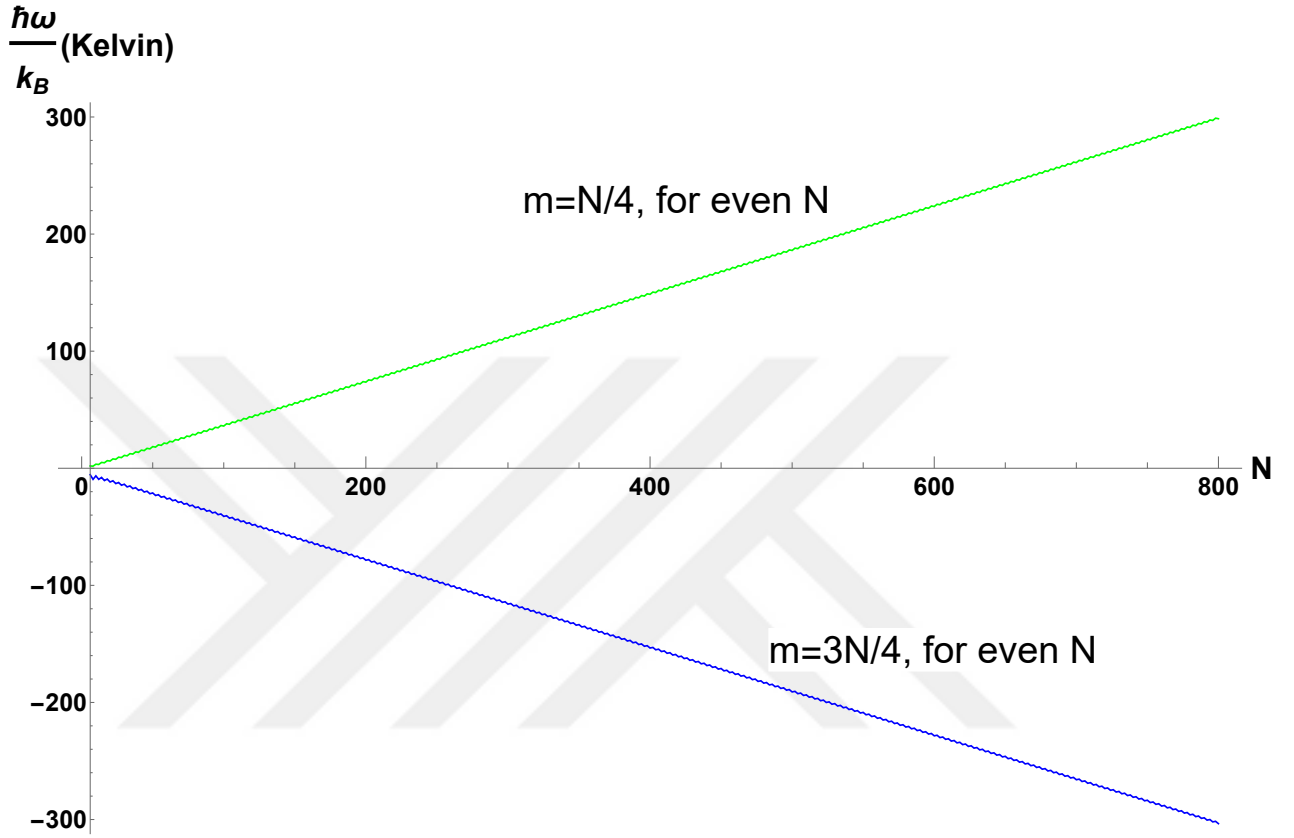
Figure 5.4: Effective temperature scaling for $m = N/4$ and $m = 3N/4$ cases, and even number of qubits in the cluster

This is because if it is located on the upper side, more states are in an excited state. As m goes away from the central region towards the edges the scaling becomes less quadratic. These are illustrated in Fig. 5.3 and Fig. 5.4. Similar graphs can be obtained for odd number of qubits in the cluster too. Therefore, it is possible to conclude that, in order to observe an advantage over just exposing the working qubit to a thermal environment, one needs to consider fuel clusters that has a biased populations of HEC blocks.

5.5.2 *Effects of Decoherence*

The results in the previous subsection are valid for ideal environmental conditions. Here we analyze how decoherence effects play role in the temperature scaling. In this case, if we denote the off-diagonal elements in the density matrix or in other words coherences as C,

due to decoherence the coherences are factorized by ξC [17]. Decoherence factor satisfies $|\xi| \leq 1$, and $\xi = 0$ corresponds to the complete decoherence, while $\xi = 1$ corresponds to the complete coherence. Since our system is surrounded by the environment, atomic relaxation and atomic dephasing effects are present. We consider three types of decoherence factors such as $\xi = \exp(-x), \xi = \exp(-xN)$, and $\xi = \exp(-xN^2)$, where $x = \gamma_\phi/\gamma$ is the ratio of atomic dephasing and relaxation rates [18]. We plot the scaling of the effective temperature of the qubit depending on the number of qubits in the cluster for three different decoherence factors. Using parameters given in [18, 17], we plot the graphs for even number of qubits in the cluster, and the graphs for odd number qubits is similar.

A.   *Figures for $m = N/2$*
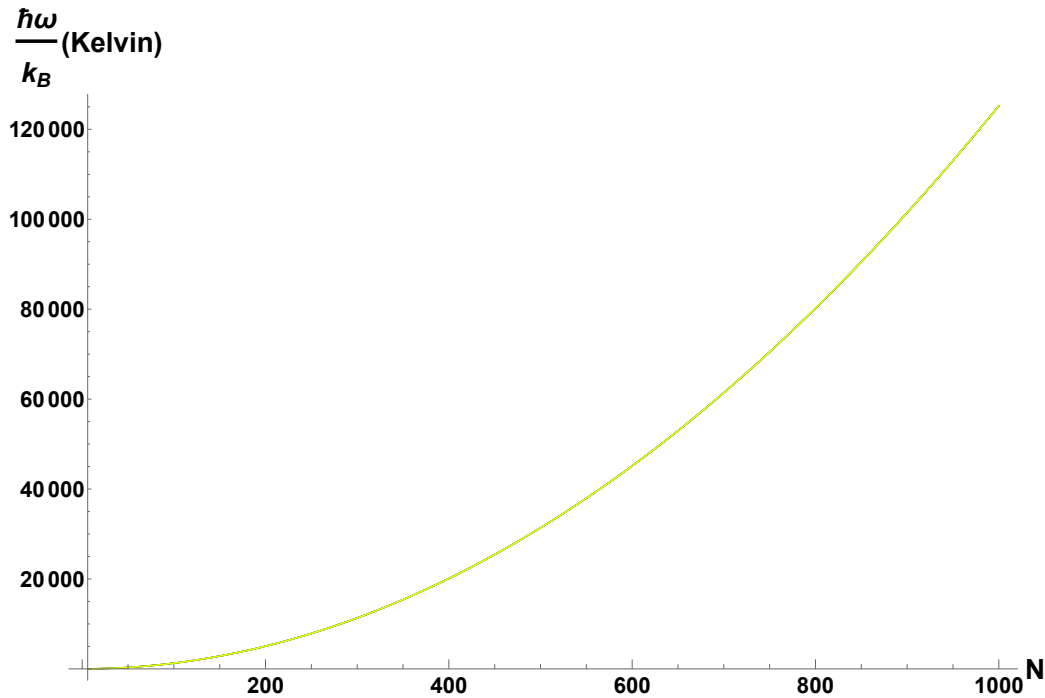
Figure 5.5: Effective temperature scaling for decoherence factor $\xi = \exp(-x)$ with $x = 0.15, 0.1, 0.05, 0.001$

(a) $\xi = \exp(-xN)$ with $x = 0.14, 0.12, 0.1, 0.08$

(b) $\xi = \exp(-xN^2)$ with $x = 0.012, 0.01, 0.008, 0.006$
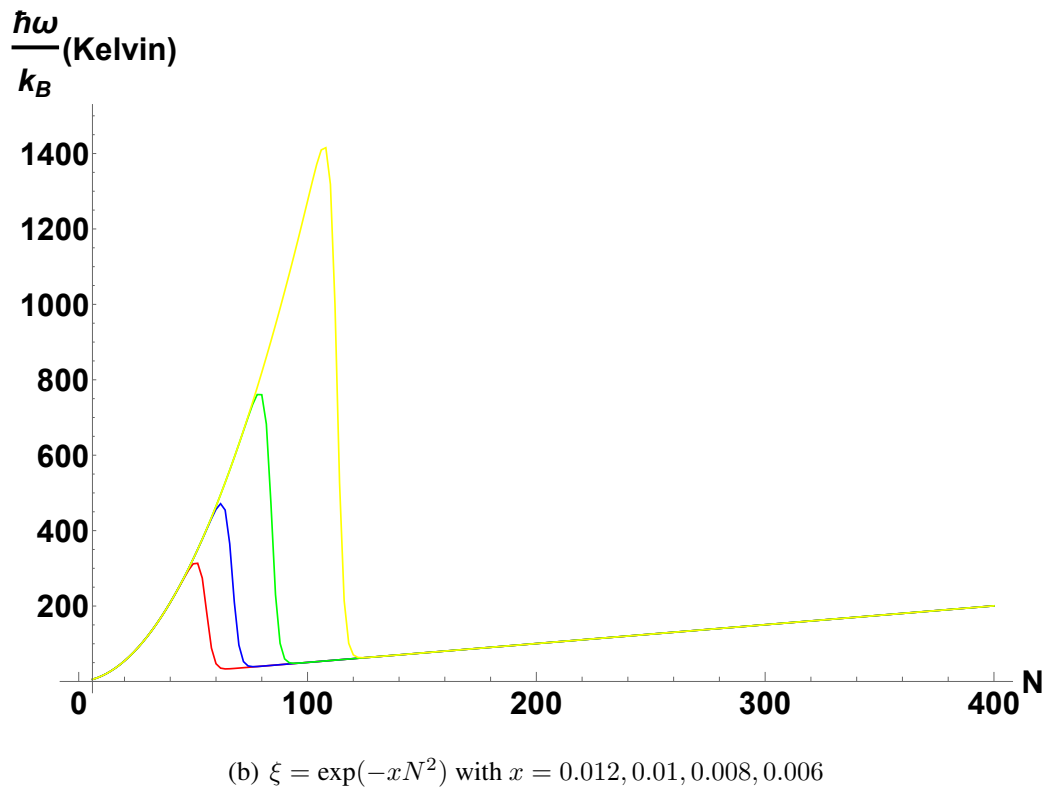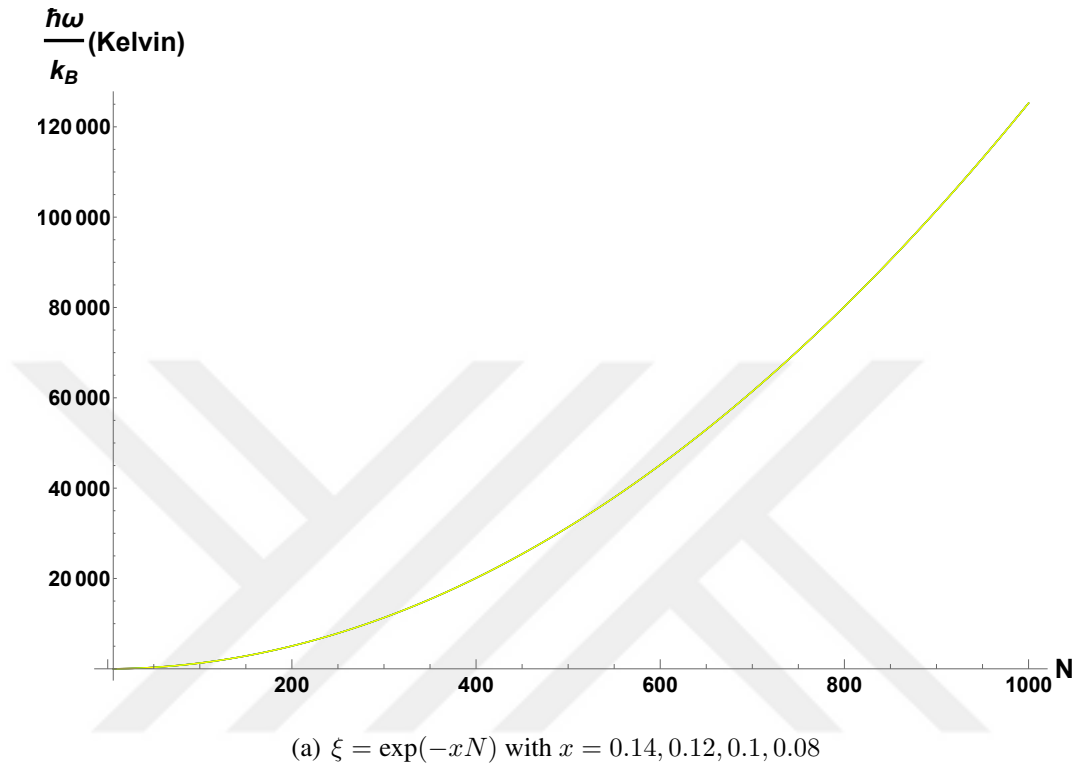
Figure 5.6: Scaling of the effective temperature

From the above figures we can observe that decoherence factor becomes important when $\xi = \exp(-xN^2)$. The scaling becomes linear instead of quadratic.

B.   *Figures for $m = N/4$, and $m = 3N/4$*
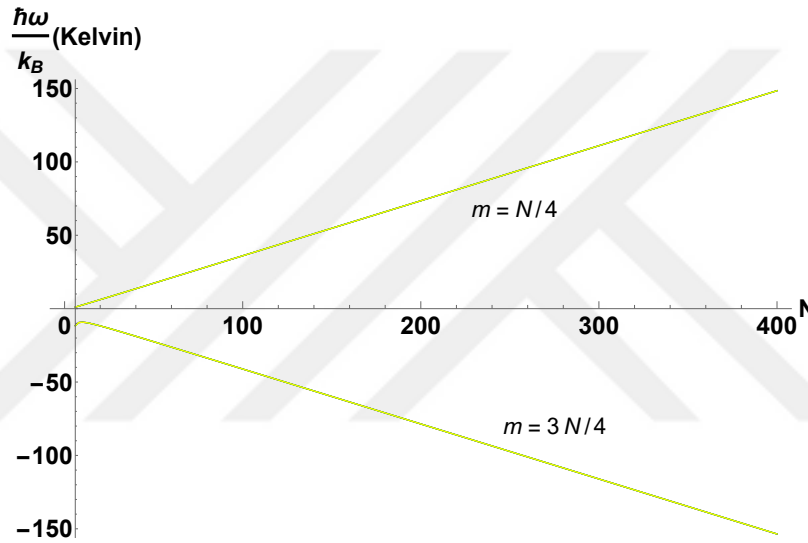
(a) $\xi = \exp(-x)$ with $x = 0.15, 0.1, 0.05, 0.001$
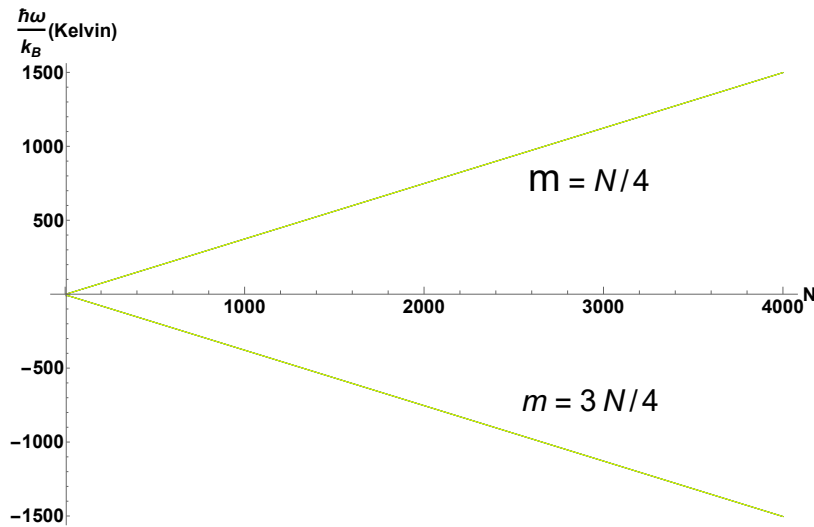
(b) $\xi = \exp(-xN)$ with $x = 0.14, 0.12, 0.1, 0.08$

Figure 5.7: Scaling of the effective temperature
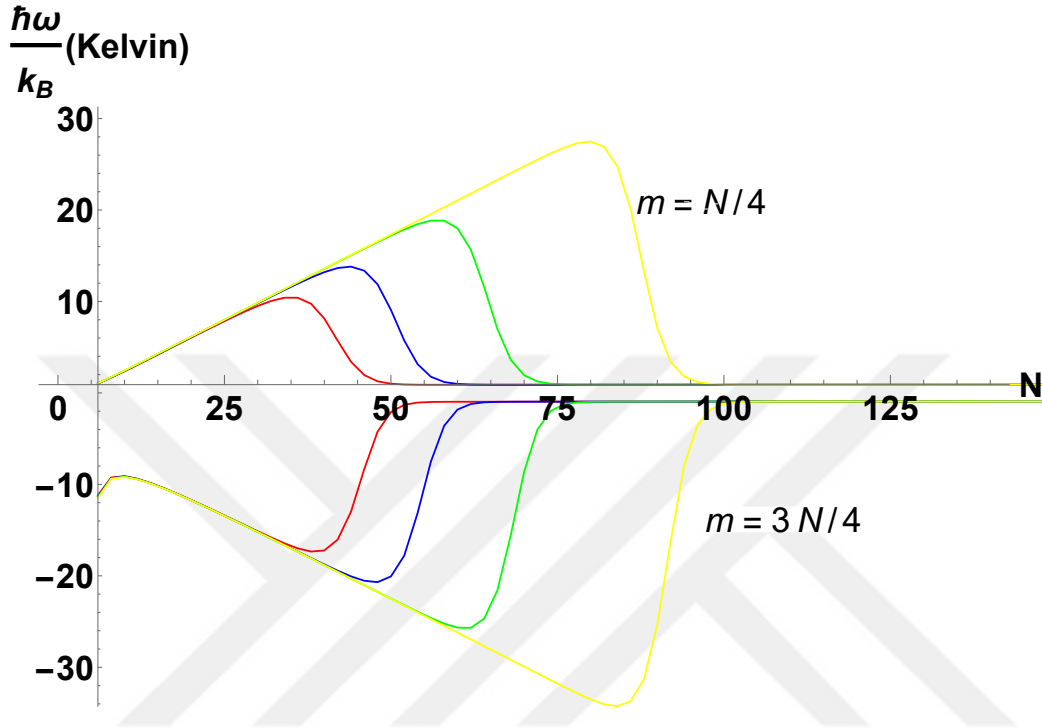
Figure 5.8: Effective temperature scaling for decoherence factor $\xi = \exp(-xN^2)$ with $x = 0.012, 0.01, 0.008, 0.006$

Decoherence factor of $\xi = \exp(-xN^2)$ also becomes important for the cases shown above. In this case, the linear scaling vanishes.

5.6 *Work Output Potential and Lorenz Curves*

We examine these coherent blocks as a resource theory. Here we consider thermo-majorization criterion as a relative distance of our athermal blocks to the thermal Gibbs state [39]. According to this criterion if we order the probabilities of the system ρ_i in the way as $p(E_1)e^{\beta E_1} > p(E_2)e^{\beta E_2} > \ldots$ in the decreasing order where β is the temperature of the system that we take as a reference, and do the same ordering for system ρ_j. Then if we plot Lorenz curves of the points $(\sum e^{\beta E_k}, \sum p(E_k))$ of each system, the transition $\rho_i \to \rho_j$ is possible if and only if the Lorenz curve of ρ_i is above the curve of ρ_j. Thermo-majorization criterion is valid for the states with cohrences too if the density matrix is positive. Athermal systems that we consider are positive, and each ρ_m state corresponds to the state with $m-1$

excitations. The ordering for ρ_m will be as $e^{\beta(m-1)\hbar\omega_0} > 0$ as the state with $m-1$ excitations has probability $p = 1$, and the Lorenz curves for each state is illustrated in Fig. 5.9.
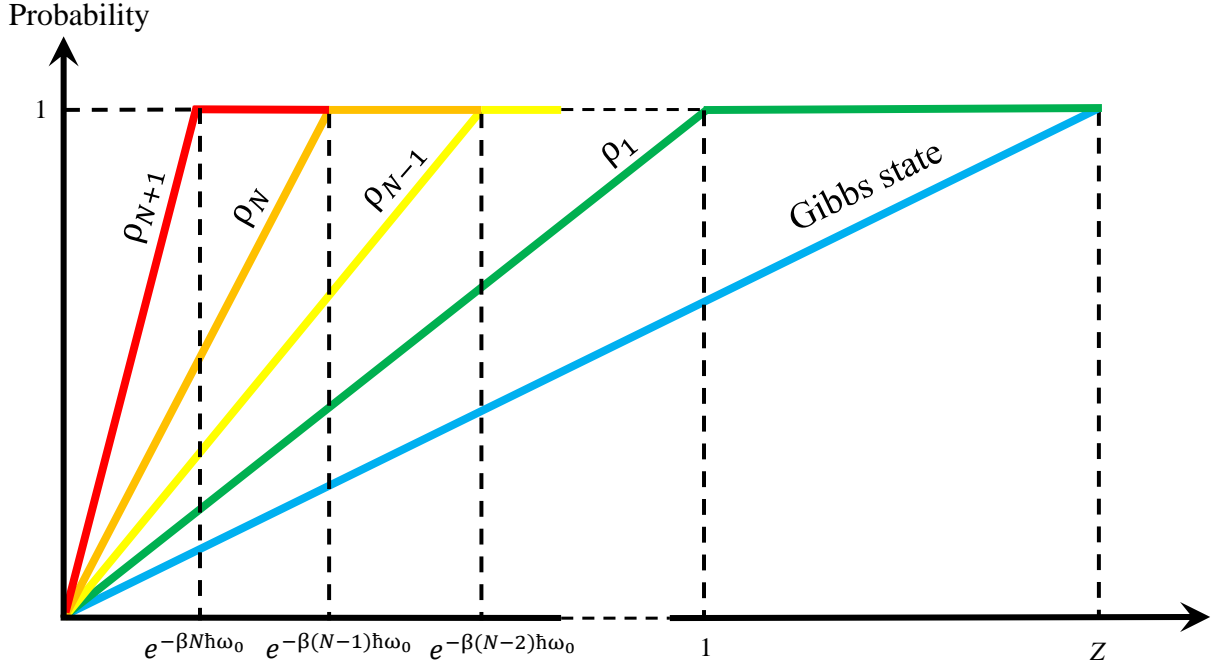
Figure 5.9: Lorenz curves for athermal states with the Gibbs state as a reference state. State ρ_{N+1} with N excitations lies above all other states. Also, thermally generated and thermally entangled states have the same Lorenz curves as the Gibbs state

Lorenz curves show the maximal work that can be obtained from the system [40]. For example, thermally generated coherent fuel has the same Lorenz curve as the Gibbs state and cannot produce additional work. Thermally entangled qubit fuels have a Lorenz curve as the Gibbs state too because they can be diagonalized to the state with an effective temperature. Athermal fuels, on the other hand, have a potential to extract useful work. However the reverse is also true in order to create such athermal states additional work must be supplied which corresponds to raising the Lorenz curve up to the desired one. This brings to a conclusion that in order to utilize the benefits of athermal states we need to pay the cost of

creating such states.

Thermally generated Dicke type of fuel is equivalent to the infinite heat bath since it thermalizes the qubit to the same temperature independent of the number of qubits in the cluster. Thermally entangled N-qubit fuel thermalizes linearly depending on the number of qubits because every qubit acts as a resource and contributes energy. The quadratic scaling for the case of athermal fuels is thermodynamically inconsistent, because we didn't take into account dephasing, and we expect the scaling to become linear too.

Chapter 6

ENGINEERING SQUEEZED THERMAL BATH

Squeezed thermal baths can enhance the efficiency of quantum heat engines and surpass Carnot bound [9, 20, 41, 42]. Because of the difficulty of embedding atom in squeezed vacuum, it is practical to engineer the atom and squeezed bath interaction [43]. In this artificial squeezed bath interaction, it is possible to observe the same effects such as the difference in the decay rates of the phase decay [44]. Here we present how we can engineer squeezed thermal bath using our model. We can mimic the same interaction if we consider the N-qubit cluster with nonzero HECs and squeezing coherences, and zero displacement coherences $\lambda = 0$. The master equation of the interaction of the single qubit with the N-qubit cluster is written as

$$
\begin{aligned}
\dot{\rho}_q(t) =& \mathcal{L}_s\rho_q + \mathcal{L}_h\rho_q = \mu(\epsilon\sigma^+\rho_q\sigma^+ + \epsilon^*\sigma^-\rho_q\sigma^-)+ \\
&+ \mu\frac{r_d}{2}[2\sigma^-\rho_q\sigma^+ - \sigma^+\sigma^-\rho_q - \rho_q\sigma^+\sigma^-] + \mu\frac{r_e}{2}[2\sigma^+\rho_q\sigma^- - \sigma^-\sigma^+\rho_q - \rho_q\sigma^-\sigma^+],
\end{aligned}
$$

(6.1)

where $\mu = p(g\tau)^2$. By using new notations $\bar{n} = r_e/(r_d - r_e), \gamma = \mu(r_d - r_e), Me^{i\phi} = -2\epsilon\mu/\gamma$, we can express the master equation in the standard form as

$$
\begin{aligned}
\dot{\rho}_q =& \frac{1}{2}\gamma(\bar{n}+1)(2\sigma^-\rho_q\sigma^+ - \sigma^+\sigma^-\rho_q - \rho_q\sigma^+\sigma^-) + \frac{1}{2}\gamma\bar{n}(2\sigma^+\rho_q\sigma^- - \sigma^-\sigma^+\rho_q - \rho_q\sigma^-\sigma^+)- \\
&- \gamma Me^{i\phi}\sigma^+\rho_q\sigma^+ - \gamma Me^{-i\phi}\sigma^-\rho_q\sigma^-.
\end{aligned}
$$

(6.2)

This master equation corresponds to the interaction of the qubit with the squeezed thermal bath with the following characteristics

$$
\begin{aligned}
\bar{n} =& N_{th}(\cosh^2 r + \sinh^2 r) + \sinh^2 r \\
M =& (N_{th} + 1)\cosh(r)\sinh(r).
\end{aligned}
$$

(6.3)

N_{th} is the effective average photon number of the bath, and r is the squeezing parameter. By choosing proper HECs r_e, r_d, and squeezing coherences ϵ, we can engineer an effective squeezed thermal bath with certain average photon number N_{th}, and squeezing parameter r. Moreover, the following inequality

$$|M|^2 \leq \bar{n}(\bar{n}+1) \tag{6.4}$$

holds [45]. This inequality ensures that the density matrix ρ_q is positive definite and trace-preserving. In order to satisfy this condition HECs and squeezing coherences should obey the following inequality

$$4|\epsilon|^2 \leq r_e r_d. \tag{6.5}$$

Chapter 7

SINGLE QUBIT HEAT ENGINE

7.1 Bloch Equations of Qubit

We first derive the Bloch equations for the qubit interacting with general non-thermal bath. In this case, all the coherences such as HECs, squeezing, and displacing coherences are present. The master equation is given as

$$\dot{\rho}_q(t) = -i[H_{\text{eff}}, \rho_q] + \mathcal{L}_s\rho_q + \mathcal{L}_h\rho_q =$$

$$= -i[pg\tau(\lambda\sigma^+ + \lambda^*\sigma^-), \rho_q] + \frac{1}{2}\gamma(\bar{n}+1)(2\sigma^-\rho_q\sigma^+ - \sigma^+\sigma^-\rho_q - \rho_q\sigma^+\sigma^-) + \quad (7.1)$$

$$+ \frac{1}{2}\gamma\bar{n}(2\sigma^+\rho_q\sigma^- - \sigma^-\sigma^+\rho_q - \rho_q\sigma^-\sigma^+) - \gamma Me^{i\phi}\sigma^+\rho_q\sigma^+ - \gamma Me^{-i\phi}\sigma^-\rho_q\sigma^-.$$

The solution to this master equation in the form of Bloch equations is as follows

$$\langle\dot{\sigma}_x\rangle = -\frac{\gamma}{2}(2\bar{n} + M + M^* + 1)\langle\sigma_x\rangle - \frac{i\gamma}{2}(M - M^*)\langle\sigma_y\rangle + \frac{1}{2}ipg\tau(\lambda - \lambda^*)\langle\sigma_z\rangle,$$

$$\langle\dot{\sigma}_y\rangle = -\frac{\gamma}{2}(2\bar{n} + M + M^* + 1)\langle\sigma_y\rangle - \frac{i\gamma}{2}(M - M^*)\langle\sigma_x\rangle - \frac{1}{2}pg\tau(\lambda + \lambda^*)\langle\sigma_z\rangle, \quad (7.2)$$

$$\langle\dot{\sigma}_z\rangle = -\gamma[(2\bar{n} + 1)\langle\sigma_z\rangle + 1] - 2ipg\tau[(\lambda - \lambda^*)\langle\sigma_x\rangle + i(\lambda + \lambda^*)\langle\sigma_y\rangle].$$

Their steady-state solution is given as

$$\langle\sigma_x\rangle_{ss} = \frac{\frac{i\gamma pg\tau}{4}[(2\bar{n} + M + M^* + 1)(\lambda - \lambda^*) + (M - M^*)(\lambda + \lambda^*)]}{d},$$

$$\langle\sigma_y\rangle_{ss} = \frac{\frac{-\gamma pg\tau}{4}[(2\bar{n} + M + M^* + 1)(\lambda + \lambda^*) - (M - M^*)(\lambda - \lambda^*)]}{d}, \quad (7.3)$$

$$\langle\sigma_z\rangle_{ss} = \frac{\frac{\gamma^2}{4}[(2\bar{n} + M + M^* + 1)^2 + (M - M^*)^2]}{d},$$

where d is

$$d = \big[(pg\tau)^2((M - M^*)(\lambda^2 - \lambda^{*2}) - 2|\lambda|^2(2\bar{n} + M + M^* + 1)) - \\ - \frac{\gamma^2(2N + 1)}{4}((2\bar{n} + M + M^* + 1)^2 + (M - M^*)^2)\big]. \tag{7.4}$$

The energy of the qubit is related to $\langle\sigma_z\rangle$. From $\langle\sigma_z\rangle_{ss}$, we see that all the coherences contribute to the final energy of the qubit. However, if there is no displacing coherences $\lambda = 0$, the steady-state energy depends only on HECs, and off-diagonal elements of ρ_q vanish. In this case, the steady-state energy of the qubit becomes

$$\langle H_q\rangle_{ss} = -\frac{\hbar\omega_q}{2}\frac{1}{2\bar{n} + 1}. \tag{7.5}$$

From this result we can observe that the squeezing coherences cannot contribute to the final energy of the qubit if the displacing coherneces are zero. In this case, the steady-state energy depends on HECs only.

7.2 Otto Cycle

We consider single qubit heat engine undergoing Otto cycle. The Otto cycle consists of four strokes, isentropic compression, hot isochore, isentropic expansion, and cold isochore. Compression, expansion, and isochoric processes imply that the working mode has a volume. However, we use qubit as a working mode. This raises a question as to how to run an Otto cycle using a single qubit. Quantum version of the first law of thermodynamics should be expressed in this case. The internal energy of the qubit is given as

$$U = \langle H_q\rangle = \text{Tr}[\rho_q H_q]. \tag{7.6}$$

The change in the internal energy is expressed as

$$dU = \text{Tr}[d\rho_q H_q] + \text{Tr}[\rho_q dH_q]. \tag{7.7}$$

This resembles the classical first law of thermodynamics

$$dU = đQ + đW, \tag{7.8}$$

and therefore we can define work and heat for quantum systems as [46, 47, 48]

$$\dbar Q = \text{Tr}[d\rho_q H_q],$$
$$\dbar W = \text{Tr}[\rho_q dH_q].$$

(7.9)

In isentropic process there is no heat exchange with the heat reservoir $\dbar Q = 0$. Using this, we can formulate isentropic process as the process with constant qubit density matrix. Similar to the classical case, the working mode does not perform work in isochoric process in quantum version. Since the Hamiltonian of the qubit depends on the transition frequency $H_q = \hbar\omega\sigma_0^z/2$, isochore corresponds to the constant transition frequency process.

N-qubit clusters at thermal equilibrium at temperature T_c will simulate effective cold thermal bath. Thermally entangled qubit clusters as shown in Sec. 5.4 will model the hot non-thermal bath. They are generated by adding HECs coherences to the N-qubit cluster at temperature T_h. Due to HECs the effective temperature of the non-thermal bath increases to T_h^*.
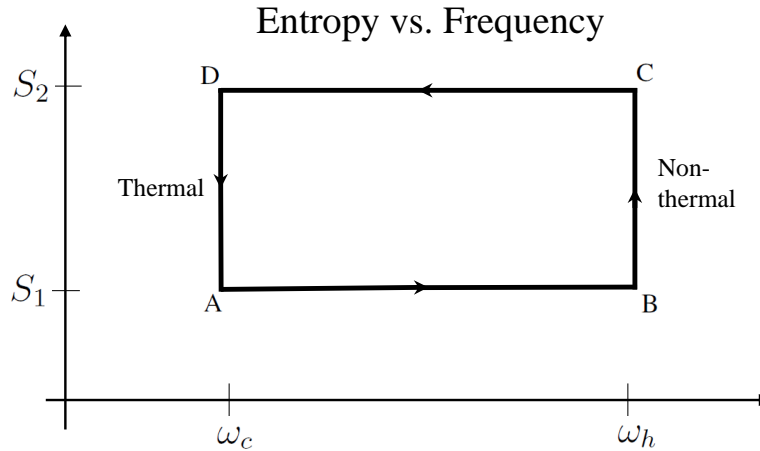
Figure 7.1: Otto cycle with single qubit as a working mode

Fig. 7.1 shows complete Otto cycle. The four strokes are described as follows:

1) Isentropic compression A → B. The qubit is initially at a thermal state in contact with

cold bath at temperature β_c and average photon number $\bar{n}_c$. Qubit's density matrix and average energy is given as

$$\rho_q = \frac{e^{-\frac{1}{2}\beta_c \hbar \omega_c \hat{\sigma}_z}}{2 \cosh(\frac{1}{2}\beta_c \hbar \omega_c)}, \qquad \langle H_q \rangle_A = -\frac{\hbar \omega_c}{2} \frac{1}{2\bar{n}_c + 1} \tag{7.10}$$

It is isentropically compressed until its frequency becomes ω_h. During isentropic process the density matrix stays constant, and the qubit's density matrix at state B is the same as in state A. Therefore, the following transition occurs

$$\langle H_q \rangle_A = -\frac{\hbar \omega_c}{2} \frac{1}{2\bar{n}_c + 1} \qquad \rightarrow \qquad \langle H_q \rangle_B = -\frac{\hbar \omega_h}{2} \frac{1}{2\bar{n}_c + 1}. \tag{7.11}$$

2) Hot Isochore B $\rightarrow$ C. The qubit is brought into contact with the hot non-thermal bath at effective temperature β_h^* with average photon number $\bar{n}_h + \Delta \bar{n}$. Qubit relaxes isochorically to the state C.

$$\langle H_q \rangle_B = -\frac{\hbar \omega_h}{2} \frac{1}{2\bar{n}_c + 1} \qquad \rightarrow \qquad \langle H_q \rangle_C = -\frac{\hbar \omega_h}{2} \frac{1}{2\bar{n}_h + \Delta \bar{n} + 1}. \tag{7.12}$$

3) Isentropic expansion C $\rightarrow$ D. The qubit undergoes an isentropic process and its density matrix stays constant during the whole expansion. Isentropic expansion changes the qubit's frequency to ω_c and the following transition occurs

$$\langle H_q \rangle_C = -\frac{\hbar \omega_h}{2} \frac{1}{2(\bar{n}_h + \Delta \bar{n}) + 1} \qquad \rightarrow \qquad \langle H_q \rangle_D = -\frac{\hbar \omega_c}{2} \frac{1}{2\bar{n}_h + \Delta \bar{n} + 1}. \tag{7.13}$$

4) Cold Isochore D $\rightarrow$ A. Finally the qubit is brought into contact with cold heat bath. Qubit then relaxes to the initial thermal state

$$\langle H_q \rangle_D = -\frac{\hbar \omega_c}{2} \frac{1}{2(\bar{n}_h + \Delta \bar{n}) + 1} \qquad \rightarrow \qquad \langle H_q \rangle_A = -\frac{\hbar \omega_c}{2} \frac{1}{2\bar{n}_c + 1}. \tag{7.14}$$

The heat received from the hot reservoir is given as

$$Q_h = \langle H_q \rangle_C - \langle H_q \rangle_B = \frac{\hbar \omega_h}{2} \frac{2(\bar{n}_h + \Delta \bar{n} - \bar{n}_c)}{(2(\bar{n}_h + \Delta \bar{n}) + 1)(2\bar{n}_c + 1)}, \tag{7.15}$$

and the heat given to the cold reservoir is given as

$$Q_c = \langle H_q \rangle_D - \langle H_q \rangle_A = \frac{\hbar \omega_c}{2} \frac{2(\bar{n}_h + \Delta \bar{n} - \bar{n}_c)}{(2(\bar{n}_h + \Delta \bar{n}) + 1)(2\bar{n}_c + 1)}. \tag{7.16}$$

Using these results, we can obtain the efficiency of the Otto engine as

$$\eta = 1 - \frac{Q_c}{Q_h} = 1 - \frac{\omega_c}{\omega_h}. \tag{7.17}$$

The efficiency of the engine depends only on the ratio of the transition frequencies. However, the efficiency is bounded by the Carnot bound. Even though the hot bath is non-thermal, we can obtain the efficiency bound by assigning an effective temperature to it [11]. As we showed in Sec. 5.4 thermally entangled fuel thermalizes the qubit to a hotter effective temperature than the thermal qubit cluster

$$\bar{n}_h + \Delta\bar{n} = \frac{1}{\exp(\frac{\hbar\omega_h}{k_b T_h^*}) - 1}. \tag{7.18}$$

The efficiency bound is given as

$$\eta \leq 1 - \frac{T_c}{T_h^*}, \tag{7.19}$$

and this efficiency bound is greater than the efficiency of the type of engine with the hot bath which is at thermal equilibrium without coherences

$$1 - \frac{T_c}{T_h^*} > 1 - \frac{T_c}{T_h}. \tag{7.20}$$

This shows that HECs can increase the efficiency bound of the quantum heat engine.

Chapter 8

CIRCUIT QED IMPLEMENTATION OF OUR MODEL

8.1 Circuit Model

In this chapter, we demonstrate how we can use circuit QED to model the interaction of the working qubit with the coherent two-qubit cluster. We use three transmons embedded in a resonator, and they are placed at the antinodes of the first harmonic. We assume that the resonator is in a vacuum state, and the transmons are strongly detuned from the resonator.
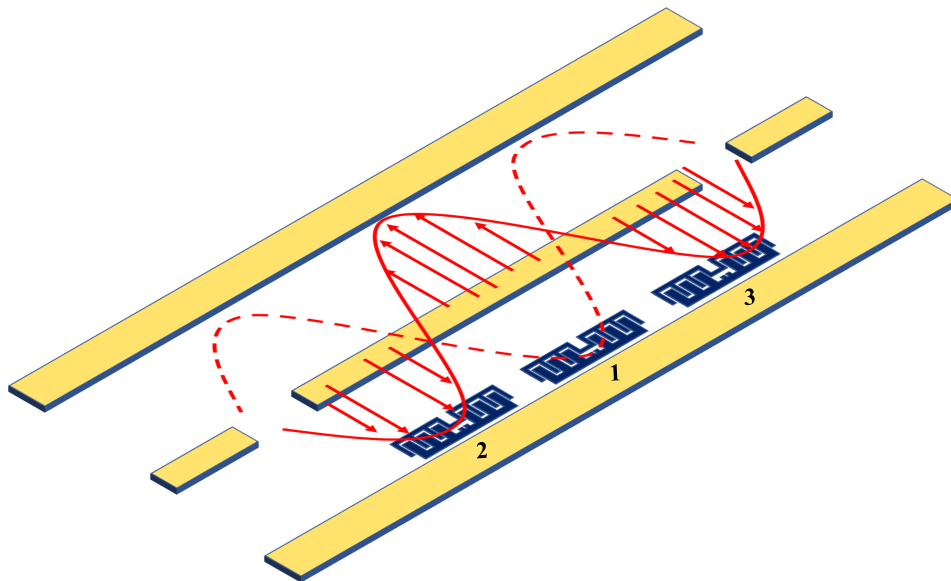
Figure 8.1: Experimental Setup.

In this case the setup can be modeled as in the Fig. 8.2 [49]. By using current coils, which control the flux through transmons, it is possible to tune the transition frequency of the qubits.
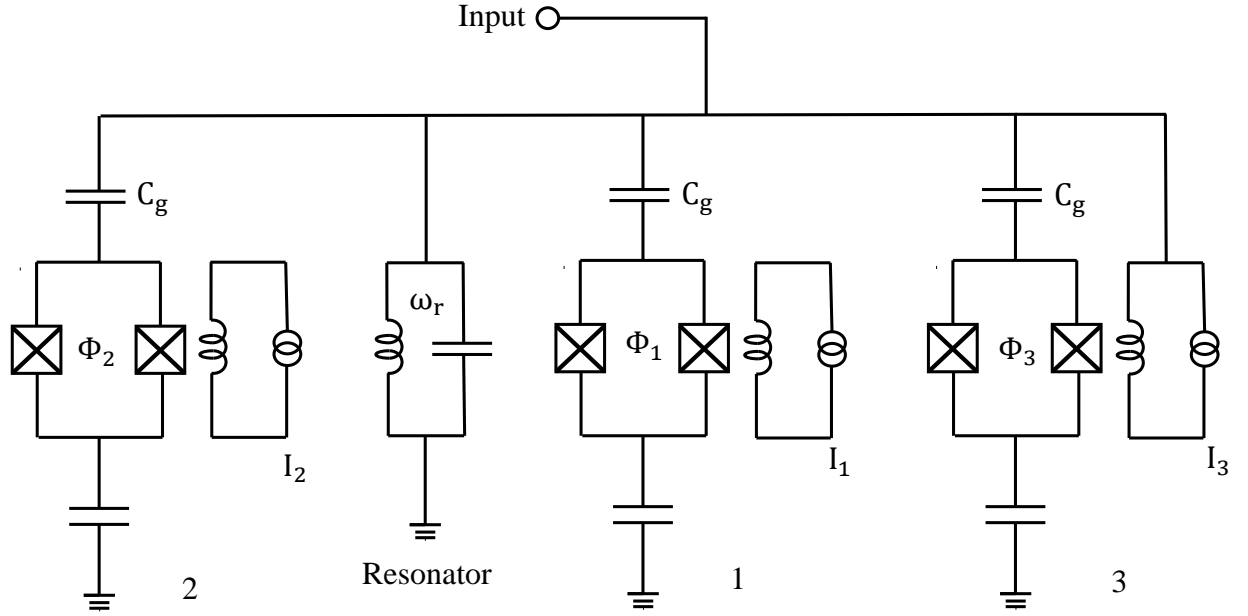
Figure 8.2: Model circuit.

The transmons are at the charge degeneracy points($n_g = 1/2$). The circuit models the interaction of the transmons with the resonator, and it can be described by the Tavis-Cummings Hamiltonian

$$H_{\text{TC}} = \omega_r a^+ a + \sum_{i=1}^{3} \frac{\omega_{ai}}{2}\sigma_i^z + \sum_{i=1}^{3} g_i(a^+\sigma_i^- + a\sigma_i^+). \tag{8.1}$$

Since the qubits are detuned from the resonator we can adiabatically eliminate the resonator-qubit interaction term using the following transformation

$$U = \exp[\sum_{i=1}^{3} \frac{g_i}{\Delta_i}(a^+\sigma_i^- - a\sigma_i^+)]. \tag{8.2}$$

Using Baker-Hausdorff formula and expanding to second order in g_i we get the following effective Hamiltonian

$$H_{\text{eff}} \approx [\omega_r + \sum_{i=1}^{3} \frac{g_i^2}{\Delta_i}\sigma_i^z]a^+a + \frac{1}{2}\sum_{i=1}^{3}[\omega_{ai} + \frac{g_i^2}{\Delta_i}]\sigma_i^z + \frac{g_1 g_2(\Delta_1 + \Delta_2)}{2\Delta_1\Delta_2}(\sigma_1^+\sigma_2^- + \sigma_1^-\sigma_2^+)+$$

$$+ \frac{g_1 g_3(\Delta_1 + \Delta_3)}{2\Delta_1\Delta_3}(\sigma_1^+\sigma_3^- + \sigma_1^-\sigma_3^+) + \frac{g_2 g_3(\Delta_2 + \Delta_3)}{2\Delta_2\Delta_3}(\sigma_2^+\sigma_3^- + \sigma_2^-\sigma_3^+). \tag{8.3}$$

This Hamiltonian is similar to the total Hamiltonian of the interaction of a pair of qubits with the working qubit, and is a valid candidate for simulation of such interaction. The frequency of the resonator is shifted by $\pm\frac{g_i^2}{\Delta_i}$, and its sign shows whether the qubit is excited or grounded. Thus it is a possible way for measuring the state of the qubits. Strong detuning of the qubits from each other turns off the qubit-qubit interaction.

Qubits 2 and 3 will model the atomic pair beam, and the qubit 1 will be the working qubit. Qubits 2 and 3 interact with qubit 1 for a short period of time τ, and then the interaction is turned off. We reset the qubit pair to the initial state. Depending on the type of interaction, the initial state of the qubit pair is either thermal state or non-thermal state. After resetting, the interaction can be turned on again, and then the procedure is repeated again.

8.2 Resetting Qubit Pair to a Thermal State

We show how the qubit pair can be reset to the thermal state. The resonator cavity can be thermalized by applying thermal radiation to its input [50, 51] as shown in the figure below.
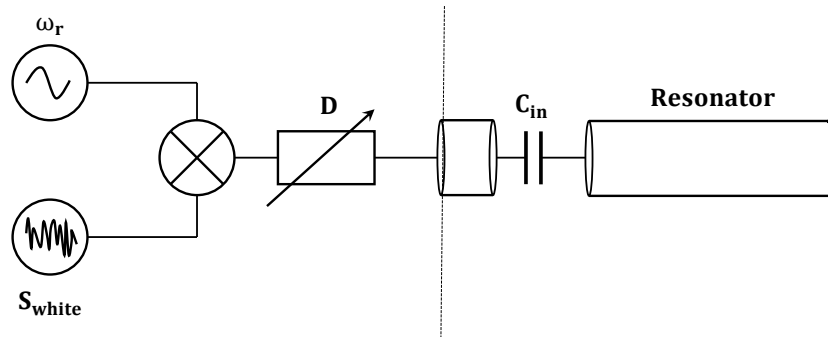
Figure 8.3: White noise source with power spectral density S_{white} is centered at the resonator frequency. It can be controlled using variable attenuation D. When connected to the input of the resonator it acts as a thermal radiation source.

This creates thermal photons in the cavity with average number given as

$$\bar{n}_{\text{th}} = \frac{1}{\exp(\frac{\hbar\omega_{\text{r}}}{k_{\text{B}}T_{\text{r}}}) - 1}.$$

(8.4)

Thus we can assign T_{r} temperature to the resonator cavity. In order to reset the transmons to thermal state we need to tune them to the resonator by changing the transition frequency. To accomplish this we send current pulse to the current coils which create flux. On resonance, the qubit reaches the thermal state at temperature of the cavity T_{r} [50]. After this we can detune the transmons from the cavity and interact them with the working qubit again.

8.3   Resetting to a Non-thermal state

We show how we can reset the qubit pairs to the thermally entangled state. We will consider the following non-thermal state

$$\rho_{\text{nth}} = \begin{pmatrix} d_3 & 0 & 0 & 0 \\ 0 & d_2 & c & 0 \\ 0 & c & d_2 & 0 \\ 0 & 0 & 0 & d_1 \end{pmatrix}.$$

(8.5)

If we diagonalize this state $U^{-1}\rho_{\text{nth}}U$ with unitary transformation given as

$$\mathbf{U} = \begin{pmatrix} 1 & 0 & 0 & 0 \\ 0 & \frac{1}{\sqrt{2}} & \frac{1}{\sqrt{2}} & 0 \\ 0 & \frac{1}{\sqrt{2}} & -\frac{1}{\sqrt{2}} & 0 \\ 0 & 0 & 0 & 1 \end{pmatrix},$$

(8.6)

we obtain the state

$$\rho_0 = \begin{pmatrix} d_3 & 0 & 0 & 0 \\ 0 & d_2 + c & 0 & 0 \\ 0 & 0 & d_2 - c & 0 \\ 0 & 0 & 0 & d_1 \end{pmatrix}.$$

(8.7)

If the coherences are less than the diagonal entries $c \ll d_2$, the diagonal state ρ_0 can be approximated as a thermal state. In the previous section, we already showed how we

can generate a thermal qubit pair. Also, any unitary matrix $\mathbf{U}$ of dimension N can be decomposed into N generalized quantum Householder reflection (QHR) matrices [18, 52, 53]. In our case, transformation matrix $\mathbf{U}$ is a four-dimensional matrix, and we need four generalized QHRs

$$\mathbf{U} = \mathbf{M}(\nu_1, \phi_1)\mathbf{M}(\nu_2, \phi_2)\mathbf{M}(\nu_3, \phi_3)\mathbf{M}(\nu_4, \phi_4), \tag{8.8}$$

where $\mathbf{M}(\nu_i, \phi_i) = \mathbb{1} + (e^{i\phi_i} - 1)|\nu_i\rangle\langle\nu_i|$. The normalized vector $|\nu_1\rangle$ and phase ϕ_1 are defined as [52]

$$|\nu_1\rangle = \frac{1}{e^{-i\phi_1} - 1}\sqrt{\frac{2\sin(\frac{\phi_1}{2})}{|1 - u_{11}|}}(|u_1\rangle - |e_1\rangle), \tag{8.9}$$

where, $|u_1\rangle$ is the first column of $\mathbf{U}$, and $\phi_1 = 2\mathrm{arg}(1 - u_{11}) - \pi$. For the rest of ν_i we take $|u_i\rangle'$ as the respective i^{th} column of $\mathbf{M}(\nu_{i-1}, -\phi_{i-1})\ldots\mathbf{M}(\nu_1, -\phi_1)\mathbf{U}$ matrix instead of $\mathbf{U}$.

For the case of unitary transformation matrix $\mathbf{U}$ given in Eq. 8.6, we obtain $\phi_1 = \phi_2 = \phi_3 = \phi_4 = \pi$, with one-dimensional phase gate as $\mathbf{M}(\nu_4, \phi_4) = \mathbf{\Phi}(0, 0, 0, \phi_4)$. The normalized vectors of QHRs are given as $|\nu_1\rangle = [0, 0, 0, 0]^T, |\nu_2\rangle = [0, -0.383, 0.924, 0]^T, |\nu_3\rangle = [0, 0, 0, 0]^T$. Standard QHRs can be implemented using magnetic pulses on flux qubits. We can realize non-thermal bath in practice with this method. After resetting, the interaction of the qubit pair with the single qubit is turned on again.

Chapter 9

CONCLUSION

We investigated how coherent N-qubit clusters can act as a non-thermal bath. These identically prepared clusters repeatedly interact with the single qubit. We showed that coherences can be classified according to their location in the density matrix of the cluster. These coherences have a disjoint contribution to the interaction with the single qubit. They can model effective thermal bath, and can coherently drive the qubit. Also, they can engineer effective squeezed thermal bath.

We focused on heat exchange coherences (HECs), and studied how they contribute to the effective temperature of the qubit. We found that HECs produced from the thermal environment cannot increase the effective temperature of the qubit more than the temperature of the thermal environment. In order to increase the effective temperature, we need to perform additional work. For example, we considered thermally entangled and athermal fuels. The former contributes to the effective temperature rise of the qubit, and the temperature scales linearly with the number of the qubits in the cluster. Athermal fuels also contribute to the effective temperature increase, and the scaling for this kind of fuel with the number of qubits is quadratic.

Furthermore, we proposed Otto engine using our model and found its efficiency. The efficiency depends only on the transition frequencies. However, we showed that the efficiency bound can increase if we add HECs to our clusters.

Finally, we proposed how we can implement our model on a circuit QED platform. We used transmons, and showed how a transmission line resonator can mediate the interaction between the qubits.

To sum up, we demonstrated that non-thermal baths are a promising resource to create efficient quantum heat engines. The main advantage of our model is that it is consisted of

qubits only, and therefore there will not be interface challenge.

BIBLIOGRAPHY

[1] Robert Alicki and David Gelbwaser-Klimovsky. Non-equilibrium quantum heat machines. *New Journal of Physics*, 17(11):115012, 2015.

[2] HED Scovil and EO Schulz-DuBois. Three-level masers as heat engines. *Physical Review Letters*, 2(6):262, 1959.

[3] Jonathan Oppenheim, Michał Horodecki, Paweł Horodecki, and Ryszard Horodecki. Thermodynamical approach to quantifying quantum correlations. *Physical review letters*, 89(18):180402, 2002.

[4] Ting Zhang, Wei-Tao Liu, Ping-Xing Chen, and Cheng-Zu Li. Four-level entangled quantum heat engines. *Physical Review A*, 75(6):062102, 2007.

[5] Raoul Dillenschneider and Eric Lutz. Energetics of quantum correlations. *EPL (Europhysics Letters)*, 88(5):50003, 2009.

[6] G Alvarado Barrios, F Albarrán-Arriagada, FA Cárdenas-López, G Romero, and JC Retamal. Role of quantum correlations in light-matter quantum heat engines. *Physical Review A*, 96(5):052119, 2017.

[7] Marlan O Scully, M Suhail Zubairy, Girish S Agarwal, and Herbert Walther. Extracting work from a single heat bath via vanishing quantum coherence. *Science*, 299(5608):862–864, 2003.

[8] Simone De Liberato and Masahito Ueda. Carnot's theorem for nonthermal stationary reservoirs. *Physical Review E*, 84(5):051122, 2011.

[9] XL Huang, Tao Wang, XX Yi, et al. Effects of reservoir squeezing on quantum systems and work extraction. *Physical Review E*, 86(5):051105, 2012.

[10] Ali ÜC Hardal and Özgür E Müstecaplıoğlu. Superradiant quantum heat engine. *Scientific reports*, 5:12953, 2015.

[11] Wolfgang Niedenzu, David Gelbwaser-Klimovsky, Abraham G Kofman, and Gershon Kurizki. On the operation of machines powered by quantum non-thermal baths. *New Journal of Physics*, 18(8):083012, 2016.

[12] CB Dag and OE Mustecaplioglu. Classification of quantum coherences for quantum thermalization. *arXiv preprint arXiv:1507.08136*, 2015.

[13] Ceren B Dağ, Wolfgang Niedenzu, Özgür E Müstecaplıoğlu, and Gershon Kurizki. Multiatom quantum coherences in micromasers as fuel for thermal and nonthermal machines. *Entropy*, 18(7):244, 2016.

[14] Jie-Qiao Liao, H Dong, CP Sun, et al. Single-particle machine for quantum thermalization. *Physical Review A*, 81(5):052121, 2010.

[15] Hai Li, Jian Zou, Wen-Li Yu, Bao-Ming Xu, Jun-Gang Li, and Bin Shao. Quantum coherence rather than quantum correlations reflect the effects of a reservoir on a system's work capability. *Physical Review E*, 89(5):052132, 2014.

[16] Deniz Türkpençe, Ferdi Altintas, Mauro Paternostro, and Özgür E Müstecaplioğlu. A photonic carnot engine powered by a spin-star network. *EPL (Europhysics Letters)*, 117(5):50002, 2017.

[17] HT Quan, P Zhang, and CP Sun. Quantum-classical transition of photon-carnot engine induced by quantum decoherence. *Physical Review E*, 73(3):036122, 2006.

[18] Deniz Türkpençe and Özgür E Müstecaplıoğlu. Quantum fuel with multilevel atomic coherence for ultrahigh specific work in a photonic carnot engine. *Physical Review E*, 93(1):012145, 2016.

[19] Obinna Abah, Johannes Rossnagel, Georg Jacob, Sebastian Deffner, Ferdinand Schmidt-Kaler, Kilian Singer, and Eric Lutz. Single-ion heat engine at maximum power. *Physical review letters*, 109(20):203006, 2012.

[20] Johannes Roßnagel, Obinna Abah, Ferdinand Schmidt-Kaler, Kilian Singer, and Eric Lutz. Nanoscale heat engine beyond the carnot limit. *Physical review letters*, 112(3):030602, 2014.

[21] Johannes Roßnagel, Samuel T Dawkins, Karl N Tolazzi, Obinna Abah, Eric Lutz, Ferdinand Schmidt-Kaler, and Kilian Singer. A single-atom heat engine. *Science*, 352(6283):325–329, 2016.

[22] Alexandre Blais, Ren-Shou Huang, Andreas Wallraff, Steven M Girvin, and R Jun Schoelkopf. Cavity quantum electrodynamics for superconducting electrical circuits: An architecture for quantum computation. *Physical Review A*, 69(6):062320, 2004.

[23] Andreas Wallraff, David I Schuster, Alexandre Blais, L Frunzio, R-S Huang, J Majer, S Kumar, Steven M Girvin, and Robert J Schoelkopf. Strong coupling of a single photon to a superconducting qubit using circuit quantum electrodynamics. *Nature*, 431(7005):162, 2004.

[24] Alexandre Blais, Jay Gambetta, A Wallraff, DI Schuster, SM Girvin, MH Devoret, and RJ Schoelkopf. Quantum-information processing with circuit quantum electrodynamics. *Physical Review A*, 75(3):032329, 2007.

[25] NV Prokof'ev and PCE Stamp. Theory of the spin bath. *Reports on Progress in Physics*, 63(4):669, 2000.

[26] M Gaudin. Diagonalisation d'une classe d'hamiltoniens de spin. *Journal de Physique*, 37(10):1087–1098, 1976.

[27] EA Chekhovich, MN Makhonin, AI Tartakovskii, Amir Yacoby, H Bluhm, KC Nowack, and LMK Vandersypen. Nuclear spin effects in semiconductor quantum dots. *Nature materials*, 12(6):494, 2013.

[28] Jun Jing and Lian-Ao Wu. Decoherence and control of a qubit in spin baths: an exact master equation study. *Scientific reports*, 8(1):1471, 2018.

[29] Friedemann Reinhard, Fazhan Shi, Nan Zhao, Florian Rempp, Boris Naydenov, Jan Meijer, Liam T Hall, Lloyd Hollenberg, Jiangfeng Du, Ren-Bao Liu, et al. Tuning a spin bath through the quantum-classical transition. *Physical review letters*, 108(20):200402, 2012.

[30] Soham Pal, Naveen Nishad, TS Mahesh, and GJ Sreejith. Temporal order in periodically driven spins in star-shaped clusters. *Physical Review Letters*, 120(18):180602, 2018.

[31] Yang Wan-Li, Wei Hua, Feng Mang, and An Jun-Hong. Tunable thermal entanglement in an effective spin-star system using coupled microcavities. *Chinese Physics B*, 18(9):3677, 2009.

[32] Michael J Hartmann, Fernando GSL Brandao, and Martin B Plenio. Effective spin systems in coupled microcavities. *Physical review letters*, 99(16):160501, 2007.

[33] AO Niskanen, K Harrabi, F Yoshihara, Y Nakamura, S Lloyd, and JS Tsai. Quantum coherent tunable coupling of superconducting qubits. *Science*, 316(5825):723–726, 2007.

[34] Barış Çakmak, Steve Campbell, Bassano Vacchini, Özgür E Müstecaplıoğlu, and Mauro Paternostro. Robust multipartite entanglement generation via cascaded interactions. *arXiv preprint arXiv:1803.05243*, 2018.

[35] Alessandro Chiesa, George FS Whitehead, Stefano Carretta, Laura Carthy, Grigore A Timco, Simon J Teat, Giuseppe Amoretti, Eva Pavarini, Richard EP Winpenny, and

Paolo Santini. Molecular nanomagnets with switchable coupling for quantum simulation. *Scientific reports*, 4:7423, 2014.

[36] Arzhang Ardavan, Olivier Rival, John JL Morton, Stephen J Blundell, Alexei M Tyryshkin, Grigore A Timco, and Richard EP Winpenny. Will spin-relaxation times in molecular magnets permit quantum information processing? *Physical review letters*, 98(5):057201, 2007.

[37] B Çakmak, A Manatuly, and ÖE Müstecaplıoğlu. Thermal production, protection, and heat exchange of quantum coherences. *Physical Review A*, 96(3):032117, 2017.

[38] Angel Rivas and Susana F Huelga. *Open Quantum Systems*. Springer, 2012.

[39] Piotr Ćwikliński, Michał Studziński, Michał Horodecki, and Jonathan Oppenheim. Towards fully quantum second laws of thermodynamics: limitations on the evolution of quantum coherences. *arXiv preprint arXiv:1405.5029*, 2014.

[40] Michał Horodecki and Jonathan Oppenheim. Fundamental limitations for quantum and nanoscale thermodynamics. *Nature communications*, 4:2059, 2013.

[41] Gonzalo Manzano, Fernando Galve, Roberta Zambrini, and Juan MR Parrondo. Entropy production and thermodynamic power of the squeezed thermal reservoir. *Physical Review E*, 93(5):052120, 2016.

[42] Jan Klaers, Stefan Faelt, Atac Imamoglu, and Emre Togan. Squeezed thermal reservoirs as a resource for a nanomechanical engine beyond the carnot limit. *Physical Review X*, 7(3):031044, 2017.

[43] N Lütkenhaus, JI Cirac, and P Zoller. Mimicking a squeezed-bath interaction: Quantum-reservoir engineering with atoms. *Physical Review A*, 57(1):548, 1998.

[44] CW Gardiner. Inhibition of atomic phase decays by squeezed light: A direct effect of squeezing. *Physical review letters*, 56(18):1917, 1986.

[45] Heinz-Peter Breuer and Francesco Petruccione. *The theory of open quantum systems.* Oxford University Press on Demand, 2002.

[46] HT Quan, Yu-xi Liu, CP Sun, and Franco Nori. Quantum thermodynamic cycles and quantum heat engines. *Physical Review E*, 76(3):031105, 2007.

[47] Tien D Kieu. The second law, maxwell's demon, and work derivable from quantum heat engines. *Physical review letters*, 93(14):140403, 2004.

[48] Philipp Strasberg, Gernot Schaller, Tobias Brandes, and Massimiliano Esposito. Quantum and information thermodynamics: A unifying framework based on repeated interactions. *Physical Review X*, 7(2):021003, 2017.

[49] JM Fink, R Bianchetti, Matthias Baur, M Göppl, Lars Steffen, Stefan Filipp, PJ Leek, Alexandre Blais, and Andreas Wallraff. Dressed collective qubit states and the tavis-cummings model in circuit qed. *Physical review letters*, 103(8):083601, 2009.

[50] JM Fink, L Steffen, P Studer, Lev S Bishop, M Baur, R Bianchetti, D Bozyigit, C Lang, S Filipp, PJ Leek, et al. Quantum-to-classical transition in cavity quantum electrodynamics. *Physical review letters*, 105(16):163601, 2010.

[51] Ali ÜC Hardal, Nur Aslan, CM Wilson, and Özgür E Müstecaplıoğlu. Quantum heat engine with coupled superconducting resonators. *Physical Review E*, 96(6):062120, 2017.

[52] Peter A Ivanov, ES Kyoseva, and Nikolay V Vitanov. Engineering of arbitrary u (n) transformations by quantum householder reflections. *Physical Review A*, 74(2):022323, 2006.

[53] James DiGuglielmo, Boris Hage, Alexander Franzen, Jaromír Fiurášek, and Roman Schnabel. Experimental characterization of gaussian quantum-communication channels. *Physical Review A*, 76(1):012323, 2007.

Appendix A

TIME-EVOLUTION OPERATOR

A.1   2-qubit fuel

$$U(\tau) = \begin{pmatrix} 1 - (g\tau)^2 \sigma_0^- \sigma_0^+ & -ig\tau\sigma_0^- & -ig\tau\sigma_0^- & 0 \\ -ig\tau\sigma_0^+ & 1 - \frac{(g\tau)^2}{2} & -\frac{(g\tau)^2}{2} & -ig\tau\sigma_0^- \\ -ig\tau\sigma_0^+ & -\frac{(g\tau)^2}{2} & 1 - \frac{(g\tau)^2}{2} & -ig\tau\sigma_0^- \\ 0 & -ig\tau\sigma_0^+ & -ig\tau\sigma_0^+ & 1 - (g\tau)^2 \sigma_0^+ \sigma_0^- \end{pmatrix}. \tag{A.1}$$

A.2   3-qubit fuel

$$U(\tau) = \begin{pmatrix} 1 - \frac{3}{2}(g\tau)^2\sigma_0^-\sigma_0^+ & -ig\tau\sigma_0^- & -ig\tau\sigma_0^- & 0 & -ig\tau\sigma_0^- & 0 & 0 & 0 \\ -ig\tau\sigma_0^+ & 1 - \frac{(g\tau)^2}{2}(1+\sigma_0^-\sigma_0^+) & -\frac{(g\tau)^2}{2} & -ig\tau\sigma_0^- & -\frac{(g\tau)^2}{2} & -ig\tau\sigma_0^- & 0 & 0 \\ -ig\tau\sigma_0^+ & -\frac{(g\tau)^2}{2} & 1 - \frac{(g\tau)^2}{2}(1+\sigma_0^-\sigma_0^+) & -ig\tau\sigma_0^- & -\frac{(g\tau)^2}{2} & 0 & -ig\tau\sigma_0^- & 0 \\ 0 & -ig\tau\sigma_0^+ & -ig\tau\sigma_0^+ & 1 - \frac{(g\tau)^2}{2}(1+\sigma_0^+\sigma_0^-) & 0 & -\frac{(g\tau)^2}{2} & -\frac{(g\tau)^2}{2} & 0 \\ -ig\tau\sigma_0^+ & -\frac{(g\tau)^2}{2} & -\frac{(g\tau)^2}{2} & 0 & 1 - \frac{(g\tau)^2}{2}(1+\sigma_0^-\sigma_0^+) & -ig\tau\sigma_0^- & -ig\tau\sigma_0^- & 0 \\ 0 & -ig\tau\sigma_0^+ & 0 & -\frac{(g\tau)^2}{2} & -ig\tau\sigma_0^+ & 1 - \frac{(g\tau)^2}{2}(1+\sigma_0^+\sigma_0^-) & -\frac{(g\tau)^2}{2} & -ig\tau\sigma_0^- \\ 0 & 0 & -ig\tau\sigma_0^+ & -\frac{(g\tau)^2}{2} & -ig\tau\sigma_0^+ & -\frac{(g\tau)^2}{2} & 1 - \frac{(g\tau)^2}{2}(1+\sigma_0^+\sigma_0^-) & -ig\tau\sigma_0^- \\ 0 & 0 & 0 & -ig\tau\sigma_0^+ & 0 & -ig\tau\sigma_0^+ & -ig\tau\sigma_0^+ & 1 - \frac{3}{2}(g\tau)^2\sigma_0^+\sigma_0^- \end{pmatrix}. \tag{A.2}$$

Appendix B

COEFFICIENTS OF THE LINDBLADIANS IN THE MASTER EQUATION

B.1 2-qubit fuel

r_e	$2a_{11} + a_{22} + a_{23} + a_{32} + a_{33}$
r_d	$2a_{44} + a_{22} + a_{23} + a_{32} + a_{33}$
λ	$a_{12} + a_{13} + a_{24} + a_{34}$
ϵ	a_{14}

Table B.1: The Lindbladian coefficients in the master equation for 2-qubit case

B.2 3-qubit fuel

r_e	$3a_{11} + 2a_{22} + 2a_{23} + 2a_{44} + a_{55} + a_{66} + a_{77} + a_{23} + a_{24} + a_{34} + a_{32} + a_{42} + a_{43} + a_{56} + a_{57} + a_{67} + a_{65} + a_{75} + a_{76}$
r_d	$a_{22} + a_{23} + a_{44} + 2a_{55} + 2a_{66} + 2a_{77} + 4a_{88} + a_{23} + a_{24} + a_{34} + a_{32} + a_{42} + a_{43} + a_{56} + a_{57} + a_{67} + a_{65} + a_{75} + a_{76}$
λ	$a_{12} + a_{13} + a_{14} + a_{25} + a_{26} + a_{35} + a_{37} + a_{46} + a_{47} + a_{58} + a_{68} + a_{78}$
ϵ	$a_{15} + a_{16} + a_{17} + a_{28} + a_{38} + a_{48}$

Table B.2: The Lindbladian coefficients in the master equation for 3-qubit case

B.3   4-qubit fuel

r_e	$4a_{11} + 3(a_{22} + a_{33} + a_{44} + a_{55}) + 2(a_{66} + a_{77} + a_{88} + a_{99} + a_{1010} + a_{1111}) + a_{1212} + a_{1313} + a_{1414} + a_{1515} +$ $+a_{23} + a_{24} + a_{25} + a_{34} + a_{35} + a_{45} + a_{32} + a_{42} + a_{43} + a_{52} + a_{53} + a_{54} + a_{67} + a_{68} + a_{69} + a_{610} + a_{78} + a_{79} + a_{711} +$ $+a_{810} + a_{811} + a_{910} + a_{911} + a_{1011} + a_{76} + a_{86} + a_{87} + a_{96} + a_{97} + a_{106} + a_{108} + a_{109} + a_{117} + a_{118} + a_{119} + a_{1110} +$ $+a_{1213} + a_{1214} + a_{1215} + a_{1314} + a_{1315} + a_{1415} + a_{1312} + a_{1412} + a_{1413} + a_{1512} + a_{1513} + a_{1514}$
r_d	$a_{22} + a_{33} + a_{44} + a_{55} + 2(a_{66} + a_{77} + a_{88} + a_{99} + a_{1010} + a_{1111}) + 3(a_{1212} + a_{1313} + a_{1414} + a_{1515}) + 4a_{1616} +$ $+a_{23} + a_{24} + a_{25} + a_{34} + a_{35} + a_{45} + a_{32} + a_{42} + a_{43} + a_{52} + a_{53} + a_{54} + a_{67} + a_{68} + a_{69} + a_{610} + a_{78} + a_{79} + a_{711} +$ $+a_{810} + a_{811} + a_{910} + a_{911} + a_{1011} + a_{76} + a_{86} + a_{87} + a_{96} + a_{97} + a_{106} + a_{108} + a_{109} + a_{117} + a_{118} + a_{119} + a_{1110} +$ $+a_{1213} + a_{1214} + a_{1215} + a_{1314} + a_{1315} + a_{1415} + a_{1312} + a_{1412} + a_{1413} + a_{1512} + a_{1513} + a_{1514}$
λ	$a_{12} + a_{13} + a_{14} + a_{15} + a_{26} + a_{29} + a_{210} + a_{37} + a_{39} + a_{311} + a_{48} + a_{410} + a_{411} + a_{56} + a_{57} + a_{58} + a_{613} + a_{614} +$ $+a_{713} + a_{715} + a_{814} + a_{815} + a_{912} + a_{913} + a_{1012} + a_{1014} + a_{1112} + a_{1115} + a_{1216} + a_{1316} + a_{1416} + a_{1516}$
ϵ	$2(a_{16} + a_{17} + a_{18} + a_{19} + a_{110} + a_{111} + a_{212} + a_{213} + a_{214} + a_{312} + a_{313} + a_{315} + a_{412} + a_{414} + a_{415} + a_{513} + a_{514} +$ $+a_{515} + a_{616} + a_{716} + a_{816} + a_{916} + a_{1016} + a_{1116})$

Table B.3: The Lindbladian coefficients in the master equation for 4-qubit case

Appendix C

RATIO OF THE SUCCESSIVE WIGNER-JORDAN BLOCK TRACES

The density matrix ρ_f, we can either be written using the product basis $|m_1, m_2, \ldots, m_N\rangle$ with $m_i = \pm 1/2$, or the total spin (Dicke) basis $|jm\rangle$ with $j = N/2$ and $m = -j \ldots j$. Note that, each m corresponds to a Wigner-Jordan block in the product basis. If initially $\rho_f(0)$ has no finite element between states of different m, then the dynamics governed by Eq. 4.1 do not mix elements with different m, meaning

$$\rho_f(0) = \sum_{jm} \rho_m^j(0)|jm\rangle\langle jm| \longrightarrow \rho_f(t) = \sum_{jm} \rho_m^j(t)|jm\rangle\langle jm|. \tag{C.1}$$

In our case, all the qubits in the cluster are initially at the ground state and therefore, only $\rho_{m=-N/2}^j = 1$. The effect of the time evolution under $\mathcal{L}(\rho_f)$ in the Dicke basis will be to thermally populate every $|j, m\rangle$ with $m = -j \ldots j$ corresponding to the temperature T such that $\rho_m^j = e^{-k\hbar\omega/T}/Z$, where k is the number of excitations and $Z = \sum_{n=0}^N e^{-n\hbar\omega/T}$, as depicted below.

Now, if we transform to computation basis by a unitary transformation, the population of every $|j, m\rangle$ state will be distributed to the corresponding Wigner-Jorden block. Hence,

the relation between the ratio of the populations of $|j, m\rangle$ and $|j, m - 1\rangle$ states is directly related to the ratio of the traces of two consecutive Wigner-Jordan blocks. These ratios can then be determined as

$$\frac{\text{Tr}[D_{i+1}]}{\text{Tr}[D_i]} = \frac{e^{[-(k+1)\hbar\omega]/T}}{e^{[-k\hbar\omega]/T}} = e^{-\hbar\omega/T} = \frac{\bar{n}}{\bar{n} + 1}. \tag{C.2}$$